STRESS DISTRIBUTION AND FAILURES IN CONCRETE SLABS

UNDER LOADS APPLIED AGAINST AN EDGE

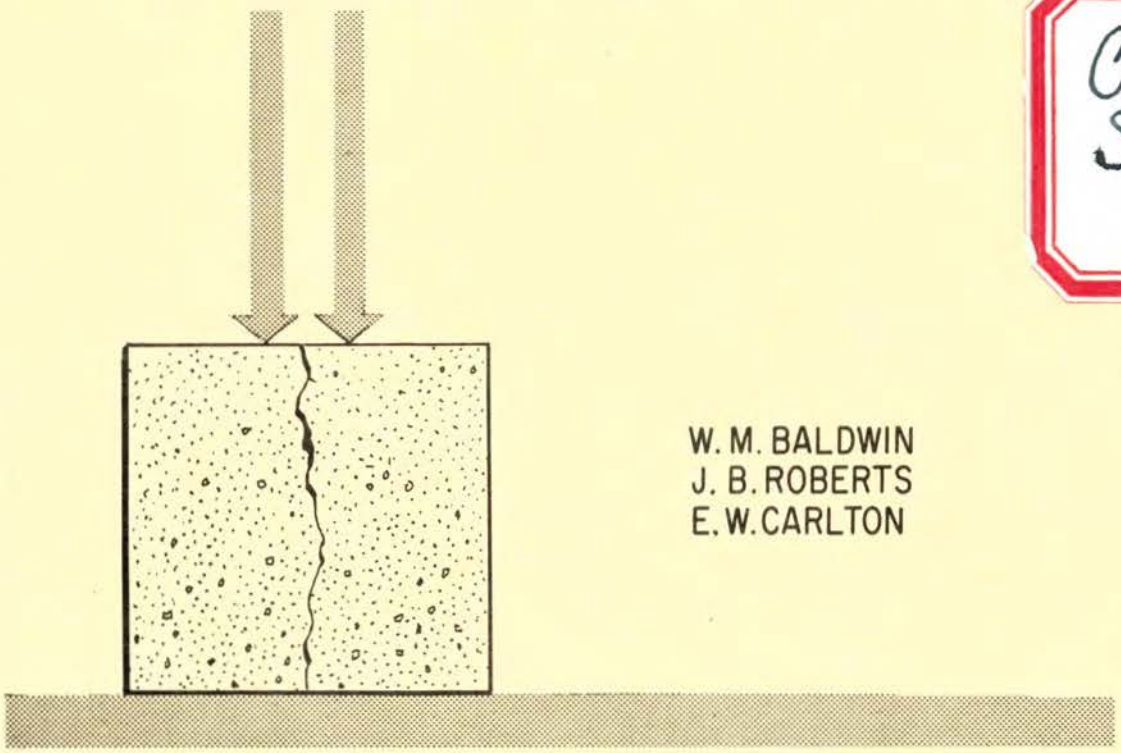

W. M. BALDWIN
J. B. ROBERTS
E. W. CARLTON

FOR THE
MISSOURI SCHOOL OF MINES AND METALLURGY
IN COOPERATION WITH
THE MISSOURI STATE HIGHWAY COMMISSION
AND
THE BUREAU OF PUBLIC ROADS
JANUARY 1961

STRESS DISTRIBUTION AND FAILURES IN THIN CONCRETE SLABS UNDER LOADS APPLIED AGAINST AN EDGE

By:

W. M. Baldwin

J. B. Roberts

E. W. Carlton

FOR THE MISSOURI SCHOOL OF MINES AND METALLURGY

In cooperation with -

THE MISSOURI STATE HIGHWAY COMMISSION

AND

THE BUREAU OF PUBLIC ROADS

January 1961

SYNOPSIS

The exploratory investigation covered by this report included a series of 27 tests to failure of thin rectangular concrete slabs under concentrated loads applied against an edge. Loads were applied at the mid-point, at the corner, and 6 inches in from the corner. Tests were made also with 2 symmetrical loads each 6 inches from the corner. The investigation included one series of slabs observed from time of loading to 50 day age, 3 slabs with one load at mid-point, and 3 slabs with 2 symmetrical loads, maintained uniformly at about 1/3 of ultimate.

All slabs were instrumented for observation of strains at various points near the loads. Strains were observed and analyzed for comparison with theoretical studies of simple radial stress distribution, of stresses in deep beams, and of stress distribution on sections of limited cross section under concentrated loads. Modes of failure obtained in the tests were local crushing failure, splitting failure in line with the loads, and edge tension failure between symmetrical loads.

Critical stress conditions for the different loading conditions are suggested. Tentative design data for the force concentrations at ends of prestressed pavements are suggested, relating to bearing stress under end anchor plates, splitting stresses on the sections in line with prestressing cables, and edge stresses between spaced end anchors.

Available published theoretical studies are reviewed in Appendixes.

INTRODUCTION

Strength properties of concrete are inefficiently utilized in conventional concrete pavements. Stresses are limited to concrete's relatively low strength in bending. As a result, thick pavements are used for high wheel loads, with corresponding increase in pavement stiffness as well. Restraints of moisture warping and temperature curling combine with load stresses to limit slab lengths, or induce critical stresses and cracking. Joints between short slabs and cracks are points for moisture attack on the subgrade and progressive deterioration in some soils. Effective use of compressive prestress holds challenging possibilities for concrete pavements through use of much longer and thinner slabs.

The application of prestressing to concrete pavements involves many unknown variables. Prominent among them are problems of continuing deformation under thin slabs and of the capacity of these slabs to resist high concentrations of forces from prestressing members at end-anchors and jacks. Many problems concerned with pavement prestressing cannot be answered without extensive field experiments and construction of actual pavements. Answers to some questions might be suggested by more modest experimental investigations.

The following problems were selected for exploratory investigations of prestressing applied to pavements in a Missouri State Highway Commission cooperative research project at the Missouri School of Mines and Metallurgy at Rolla:

A. Continuing length changes and deformations of simulated, relatively short, prestressed pavement slabs on a typical highway subgrade.

B. Physical properties of pavement concretes at early age and at different ambient temperatures, for determination of earliest age of prestressing, and possible pavement stresses prior to prestressing.

C. Stress distribution and concrete failure determination near concentrated loads applied against an edge of a thin concrete slab, in the manner longitudinal prestressing forces might be applied against ends of long prestressed slabs.

This report covers the last mentioned experimental investigation. The tests were exploratory, and have suggested some critical stress conditions, but they did not include all variables and did not establish general limits of validity. They have

particular application to wide spacing of large edge forces, such as might be expected with the smallest practical number of longitudinal prestressing cables in wide pavement lanes.

RESEARCH PROGRAM

OBJECTIVES:

Prestressing of concrete pavements very likely may involve application of spaced concentrated forces against ends and/or edges of relatively thin pavement slabs, approximately centered vertically on the section of the pavement, which can be assumed unlimited in the direction of the forces. The force concentrations may be in the form of end anchorages of prestressing cables or support for prestressing jacks.

Three critical conditions could be visualized with spaced concentrated edge forces against concrete slabs:

A. "Crushing" of the concrete in bearing at the force application points;

B. Tension stresses along the edge, evidenced as cracks between the force application points perpendicular to the edge;

C. Tension stresses some distance away from the edge, perpendicular to the direction of force application, resulting in "splitting" of the concrete along the lines of force application. (In conventional prestressed concrete this zone is generally referred to as "bursting zone".)

The investigation was intended to explore the existence and severity of these critical stress conditions, particularly with respect to influence of location of force application in relation to pavement slab corners, and to limiting stress concentrations near the forces. A limited amount of information was obtained on critical tension stresses between 2 loads. To simplify the experimental program only one size of rectangular bearing area was used, so shaped that the force was distributed evenly across the slab thickness. The slabs were as large as experimental facilities would permit and the bearing areas narrow so that conditions of simple radial stress distribution in a semi-infinite plane body were simulated closely, at least in short-time tests to failure, for concentrated perpendicular force applied at a corner and elsewhere along an edge.

It was desired, further, to obtain some indication of creep effects under long-time application of concentrated edge forces.

It was anticipated that creep in the concrete under high compressive stress near the force application points might change the normal radial stress distribution and possibly induce critical tension on each side of the bearing. Accordingly, a series of long-time load tests were included to give exploratory indications of changes in concrete strains under lasting edge forces.

TEST SPECIMENS AND TESTING ARRANGEMENT

All tests were made on 48 inch long 36 inch high and 4 inch thick concrete slabs. The loads were imposed vertically against the 48 inch long edge through steel blocks one inch thick 4 inches wide across the edge and 2 inches along the edge. A 1/4 inch pad of plywood between the steel block and the concrete aided in even distribution of force, centered on the 4 inch wide and 2 inch long blocks.

Short-time Tests were made in a 200,000 pound Olsen Universal Testing Machine with high head room. The slabs were placed on edge in the machine, with a 48 inch long, 4 x 3/4 inch piece of plywood under the slab on the steel loading platform. Loads were applied in 5,000 and 10,000 pound increments with strain readings at each load increment to failure. The short-time tests to failure included:

One load at center of the 48 inch edge, 9 slabs tested, 3 at 14, 42, and 84 day age, each;

One load immediately adjacent to one corner, 9 tests on 5 slabs, 3 at 14, 42, and 84 day age, each;

Two loads, centered 6 inches from each corner, 6 slabs tested, 3 at 14 and 42 day age, each.

One load, centered 6 inches from one corner, 3 slabs tested at 84 day age.

A test specimen in place in the testing machine is shown in Figure 1.

Long-time Loading Tests were made on specimens of the same size and with identical load blocks used in the short time tests. In these tests both 48 inch edges were loaded with directly opposed loads which were applied with hydraulic jacks, and thereafter maintained constant by a heavy coil spring behind one of the 2 opposed load blocks. The spring was held compressed by rods on each side of the slab, in the plane of opposed loads, and heavy back up plates. Figure 2 shows the testing arrangement for center loads.

In the long-time tests concentrated loads of 20,000 pounds were applied at each load point. On 3 slabs center loads were imposed and on 3 slabs symmetrical loads centered 6 inches from each corner against the 48 inch edge. Strains under load were observed for a period of 50 days. The slabs were about 4 months old at time of loading in early June. During the loading period the slabs were stored in a basement room with temperature from 71 to 78 F, average 76 F, and humidity from 66 to 91 percent, average 82 percent. The high humidity in the relatively cool summer storage may have affected the slabs and the gages so as to limit indications of the long time tests, especially during the latter part of the observation period.

Material. Concrete for all slabs was non air-entrained mix, proportioned 1:2.4:3.2 on dry weight basis, with 75 percent surplus mortar, and cement factor 6.1 sacks per cubic yard. Water cement ratio averaged 5.7 gallons per sack and slump was 3 ± 1/2 inch. The mix was designed to be typical of concrete in Missouri highway pavement construction. To decrease somewhat probable variations in strain gage readings, however, the maximum size of coarse aggregate was limited to 3/4 inch. The coarse aggregate was crushed limestone, with gradation:

0	percent retained on 3/4 inch sieve
10	percent retained on 1/2 inch sieve
35	percent retained on 3/8 inch sieve
50	percent retained on # 4 sieve
100	percent retained on #10 sieve

Concrete cylinder compressive strengths averaged:

at 14 days:	3,000 psi
at 28 days:	3,300 psi
at 42 days:	3,500 psi, (estimated)
at 84 days:	3,600 psi, (estimated)

Modulus of rupture of concrete beams 6 x 8 x 36 inches, tested with the 8 inch dimension vertical on 30 inch span for third-point loading, was:

at 14 days	520 psi
at 28 days	570 psi

Tension tests were obtained also from diametric compression tests on concrete cylinders. These gave the following average values of tension strength:

at 14 days	290 psi
at 28 days	330 psi

The Modulus of Elasticity in millions of psi secant to 50 percent of ultimate strength, was:

at 14 days, average 3.75, maximum 4.6, minimum 2.5
at 28 days, average 4.5, maximum 5.6, minimum 2.9
at 42 days, average 4.9, maximum 5.6, minimum 3.8
at 84 days, average 5.25, maximum 6.0, minimum 4.3

The slabs were cast in flat position. Concrete was mixed one minute dry, and 2 minutes wet, in a 2 cubic foot mortar mixer, placed direct into the plywood forms and vibrated in place. Four batches were used for each slab. The concrete was screeded and steel troweled smooth. The slabs were left in the forms for 7 days, curing under wet burlap, and were then stored on edge in the laboratory to the time of testing.

INSTRUMENTATION

All slabs were provided with bonded wire resistance strain gages, applied in principal directions near the loads and parallel to the loaded edges; all principal gages applied to the faces of the slabs. SR-4 gages with 13/16 inch active lengths were used, Type A-1 linear gages along the edges, parallel to them and one inch away. Strain rosette gages, Type AR-1 were used away from the loaded edge. Temperature compensation gages were placed on the slab top edge in transverse direction.

Typical views of gages in place, prior to load application, are shown in Figure 3. Dimensional diagrams showing orientation and identification of the gages are shown in Figure 4, for center load, corner load, and load 6 inches from the corners.

The slabs were dried for at least 2 days prior to attaching the gages. The area where gages were to be placed was ground smooth with a carborundum wheel, carefully brushed and dusted, then cleaned with SR-4 cleaning solvent. A liberal coat of SR-4 cement was applied, followed by solvent which softened the cement and aided in filling any irregularities remaining in the concrete surface. A second coat of SR-4 cement was applied, drying for 24 hours before the gages were applied. The slabs for long-time loading tests, after attachment of the gages and drying, were further moisture proofed by spray application of 2 coats of Acrylic plastic over the gages and soldered connections as precaution against humidity. In the long-time tests, as a precaution, both faces of the slabs were moisture proofed, although gages were applied to one face only.

The relatively short 13/16 inch active gage length was intended to give accurate orientation strain readings with respect

to distance and directions of strains, near the loads. Conversely, large variations in strain readings were to be expected, attributed to influence of coarse aggregate immediately adjacent to many gages and mortar only adjacent to others; however, the substantial number of slabs and duplicate gages could be expected to produce average values in good agreement with concrete properites. Average strains were found to be in good agreement with theory on those gages permitting close comparison between theory and observation. The use of longer gages would not have permitted observation of strains, which change greatly near the load, with close relation to orientation and distance from the load.

THEORETICAL CONSIDERATIONS

The specific structural features of loads against ends of long prestressed slabs, such as imposed by end anchorages, is the unlimited extension of the slab in the direction of the loads, and two-dimensional stress considerations in the thin slab. Some distance from the ends, stresses must of necessity be evenly distributed across the slab width, irrespective of load concentrations at the ends. Near the ends, stresses are determined by local distribution away from concentrated loads, and by stress distribution in a continuous band of concrete along the edge, acting as a continous beam of undetermined depth loaded with evenly distributed pressure at its interior edge and by equal and opposed concentrated loads as reactions at the edge.

Critical stresses have been considered in relation to theories for:

A. Formation of shear wedges due to shear failures under and near the concentrated load bearings, characteristic of local crushing;

B. Splitting below the shear wedges along the planes of loading across the slab, due to tension stresses on the mid-sections of the reactive loads, considered as a continuous deep beam;

C. Cracking perpendicular to the edge between the concentrated loads, due to bending stresses in the span of the continuous deep beam.

All these stress considerations were pertinent to the tests, and to loading conditions at the ends of prestressed slabs.

Recognized theories of two-dimensional plane stress distributions for concentrated loads have been compiled and developed by Timoshenko(1). Applications of those theories to the specific stress conditions are given in Appendix A.

For appraisal of stresses on sections perpendicular to the loaded edge, either in line with the load some distance away from the edge or between 2 loads along the edge, several studies of stresses in deep beams have been compared in Appendix B.

Shear Wedge Failure. For loads much below failure, theories for simple radial distribution of concentrated loads give excellent agreement with observations near the loads. As local failure near the load approaches, strains near the load are influenced by plastic adjustments; however, further away from the load, stresses are still nominal and stresses remain in close agreement with simple radial distribution up to failure. The theoretical stress orientation can be used as guide to the local extreme stresses if plastic adjustments are considered to average the stresses along critical failure planes, for non-brittle failure.

In Appendix A, based on theoretical simple radial distribution, the probable orientation of planes with critical average shear stress has been computed, and the average shear stress has been given, Equation (7). If shear failure is assumed to occur for average shear stress equal to one half of the concrete cylinder strength, in accordance with accepted theory for cylinder failure, the ultimate bearing pressure prior to shear wedge failure can be estimated to approach twice the cylinder strength, Equation (8). Because of the continuing plastic readjustments in the confined space the shear wedge can be expected to have fairly sharp apex angle.

Corner Load Stresses. For load at a corner, local shear failure, according to Appendix A, should occur for a bearing pressure equal to the cylinder strength directly under the bearing. In addition, for corner loads tension stresses occur along the loaded edge for some distance away from the corner. In Appendix A these stresses are given for load at the corner, and - for load a short distance away from a 90 degree corner - Equation (14) by which the stresses may be appraised. If the load p per inch thickness acts at a distance t in from the corner and parallel with the edge, the maximum tension stress along the edge is at 4t distance from the corner, and equal to about

---

(1) S. Timoshenko, Theory of Elasticity, McGraw-Hill Book Company, Inc., 1934.

0.17 p/t. For a load distributed over a bearing c immediately adjacent to the corner the load can be assumed concentrated at its mid-point c/2 from the corner, in which case the maximum stress 0.34 p/c occurs immediately inward from the bearing, substantially without decrease to 2c distance from the corner.

Appreciable tension along the loaded edge can occur only if the slab has sufficient dimensions, or other loads away from the corner, to bring reactive forces into effect; otherwise the stresses near corner loads cannot occur in accordance with simple radial distribution, and are instead concentrated in the direction of the load. Similarly, occurrence of tension cracks perpendicular to the edge inward from the corner load need not lead to collapse, as long as the load can be carried in bearing at the corner.

Splitting Failures. As long as the shear wedge forces are confined within the surrounding concrete bearing pressures should not precipitate failure; however, when the tension on mid-section below the wedge can no longer confine the bursting the concrete will split as a tension failure along the loaded plane. Although simple radial distribution of concentrated loads against an edge indicate no tension stresses on the mid-section, such stresses must arise as sectional reaction to the compression within the shear wedge. The distribution and magnitude of these sectional stresses have been derived from studies of stress distribution in deep beams.

Stresses in wall-like girders with variously concentrated supports have been studied by Dischinger[2], covered in a publication of the Portland Cement Association[3]. Similar stress problems, with specific reference to stresses in end blocks of prestressed structural members have been studied in some detail by Guyon[4], and with reference to bridge pier stresses by Bleich (5). Bleich's computations have been applied to end block stresses

---

(2) Franz Dischinger, Beitrag zur Theorie der Halbscheibe und des Wandertigen Balkens, Publications International Association for Bridges and Structural Engineering, First Volume, 1932, p. 69.

(3) Design of Deep Girders, Portland Cement Association, ST 66, 1951.

(4) Y. Guyon, Prestressed Concrete, John Wiley & Sons, New York, 1953.

(5) F. Bleich, The Column of Rectangular Section as a plane problem, (in German), Der Bauingenieur 1923, Nrs. 9 and 10.

in prestressed members by Ban, Muguruma, and Ogaki(6). Principal applicable data of all these studies have been included in Appendix B.

In accordance with two-dimensional plane stress distribution concentrated loads against an edge can be considered evenly distributed on sections at a distance from the edge equal to or greater than the spacing of the loads, or the available effective width of distribution. Beyond that distance there are no appreciable transverse stresses.

The maximum tension stresses on the mid-sections of the loads are dependent upon the length of bearing c. For effective width of load distribution, a , of loads p per unit of thickness, Dischinger established the following approximate stresses, and their distance from the loaded edge:

for c/a =0 maximum tension 0.65 p/a, at 0.20a distance from edge
for c/a =1/10 maximum tension 0.60 p/a, at 0.25a distance from edge
for c/a =1/5 maximum tension 0.52 p/a, at 0.30a distance from edge

These values are in substantial agreement with computations according to Bleich equations. Stresses suggested by Guyon are some 25 percent lower.

The total tension on the mid-sections is nearly equal in the 3 studies:

for c/a = 0 , 0.30 p
for c/a = 1/10, 0.25 p
for c/a = 1/5 , 0.20 p

Zero stress on the mid-sections of the concentrated loads, with tension on the sections at greater distance, has been found at different distances from the loads, as follows:

	By Dischinger:	By Guyon:	By Bleich:
for c/a - 1/20	1.0 c	--	1.5 c
for c/a - 1/10	0.7 c	0.9 c	1.0 c
for c/a - 1/5	0.5 c	0.6 c	0.7 c

(6) S. Ban, H. Muguruma, and Z. Ogaki, Anchorage Zone Stress Distributions in post-tensioned concrete members, Proceedings, World Conference on Prestressed Concrete, July 1957, San Francisco, California.

It is possible that shear wedge formation, rather than load spacing relations, governs the distance from the concentrated loads at which tension on the mid-section begins, between 1.0 c and 1.5 c away. Increasing bursting compression within the shear wedge would then also increase the tension stresses on the mid-section.

Edge Stresses. Tension stresses along the edge between loads against the edge are obtained from studies by Dischinger[2] and [3], given in Appendix B, for the specific case of 2 loads applied near the corners of an edge also from Guyon[4], and from the study of corner load stresses in Appendix A.

Between loads, p per unit of thickness, spaced distances a apart, against the edge of a slab of unlimited extension from the loaded edge - continuous spans - the tension stress along the edge equals 1.0 p/a , and in units of the evenly distributed prestress q , the tension is 1.0 q . The stress decreases at nearly linear rate to zero at a distance of 0.20 a from the edge.

For 2 loads against an edge of length L , each applied near the corner - single span - , the edge tension stress at the center of the edge could become 1.2 q (Ref. 3), to 1.36 q (Appendix A) according to different studies, with zero stress up to 0.35 L distance away. The total tension on the portion between the edge and the zero-stress would be 0.35 to 0.40 p .

TEST RESULTS

FAILURE LOADS

Only the short-time tests were carried to failure. Ultimate loads and modes of failure for all the specimens are given in Table 1. Slabs were selected for testing method and different ages by randomization. The different conditions of loading are listed separately, and the slabs are grouped by age at testing.

Comparing loads at failure for different ages, no significant increase in ultimate loads is noticeable from 14 to 84 day age. Averaging the results for all 3 ages, the loads at failure p_{ult} on the 2 inch long bearing, per inch of slab thickness, are found to be:

Single load at center	15,100 lb per in width
Single load 6 inches from corner	15,900 lb per in width
Single load corner	6,680 lb per in width
Two loads, each 6 inches from corner	7,040 lb per in width, each

Figure 5 shows slab condition after failures for single load at center, 6 inches from corner, and at corner. Crushing of the

concrete under the loads was a common characteristic of these failures. The views show a "shear wedge" formed below the load block, with indications of local failure a short distance out from the block as well.

For the single load at center of the edge the shear wedge was accompanied by a vertical splitting crack. For the single load 6 inches from the corner the shear wedge is more noticeable in the face of the slab. For both the corner load and the single load 6 inches in, the vertical crack formed at the inner edge of the load block, and the crack veered away slightly from the side edge with increasing depth. For the load 6 inches in, the "vertical" crack may have been a splitting crack following shear failure.

For corner load the shear wedge extends to the edge. The "vertical" crack at the inner edge of the load block appeared before development of the shear wedge.

The failure at the center of the slab for 2 loads, each centered 6 inches from the corner, Figure 6, is an obvious tension failure in flexure caused by bending of the 48 inch long and 36 inch deep beam between the 2 loads 6 inches in from the corner. For the substantial depth it would be reasonable to assume radial distribution of stress in accordance with Figure 18 and neutral axis .25 L , or 12 inches below the top edge.

CRITICAL STRESSES AT FAILURE

In Table 1 the critical stresses for average failure loads at each age have been computed in accordance with equations in Appendices A and B. These stresses will be compared with probable limits obtained from physical properties of the concrete.

Shear Wedge Stress. The average shear stress characteristic for shear wedge failure under the loading along the edge, including one load 6 inches from the corner, was 1900 psi. Compared to an average cylinder strength f'_c of 3500 psi, that is $0.55\ f'_c$. The shear wedge theory gives shear stress in close agreement with expected failure of $f'_c/2$ for the assumed shear planes at 26-1/2 degree angle with the mid-section, or somewhat steeper. For the corner load the average shear stress was 1670 psi which equals $0.48\ f'_c$. The shear wedge failure stress for corner load is in very close agreement with theoretical shear failure at $f'_c/2$.

For load away from the corner the computed shear stress at shear wedge failure is somewhat above $f'_c/2$; however, if the assumed horizontal distribution length "S" of the concentrated force were increased from actual bearing 1.0 inch by a small fraction of an inch, the computed average ultimate shear stress would be in agreement with the two-direction compressive stress

condition existing below the load. The severed shear wedge, Figure 5, has an included angle between 40 and 50°, and extends some 3 to 4 inches below the bearing, indicating failure shear planes extending between 1 and 1-1/2 inches on each side of the mid-section at the edge. Load capacity, estimated on average shear, Equation (8) is accordingly on the conservative side, according to these tests.

Splitting Tension. The theoretically derived maximum tension stress on the mid-section below a single load, 0.65 p/L does not exceed 210 psi in the tests, Table 1. This stress is not sufficient to explain the typical splitting crack which progressed from the top down in the test slabs based on deep-beam stress distribution. Bottom tension, such as might be deduced in a shallow beam is not believed to have been a cause of failure. Frictional restraint at bottom and concentration of support under central portions of the slab edge, would decrease flexural moment effectively in the tests of this investigation. No appreciable flexural tension would be present for the load 6 inches from the corner.

Splitting failure is believed to have been secondary to the shear wedge formation, and caused by high horizontal pressure incident to confined vertical displacement of the shear wedge during initial failure. Such wedge forces would result in very high horizontal tension stresses immediately below the shear wedge; however, there is no equation for this stress concentration available. Wedge bursting forces might have been counteracted to some extent by flexural compression for load at the center of the edge, but no substantial flexural compression would be present under the single load 6 inches from the corner. The secondary splitting failure accordingly, does not appear to vary greatly with compressive stress in the range of these tests on the section at the load.

Corner Tension Stress. The maximum corner tension stress, Table 1, according to Equation (3) is higher than either modulus of rupture or tension strength of the concrete; however, high tension stresses could occur only very near the distributed corner load in these tests, because equalizing moments beyond the normal critical sections were lacking in the 4 foot long test slabs. The tension immediately beside the 2 inch long corner load was undoubtedly sufficient to cause cracking perpendicular to the edge prior to shear failure under the load.

Tension Stress between Symmetrical Loads. The computed tension stress at the mid-section between 2 loads each 6 inches from the corner, average 420 psi, Table 1, agrees well with the tension strength indicated by the cylinder splitting test, although lower

TABLE 1. FAILURE LOADS AND APPROXIMATE CRITICAL STRESSES AT FAILURE OF EDGE LOADED SLABS.

Slab No.	Age days	Ultimate Load: At Each Point: Pound	Ultimate Load: At Each Point: Pound Per Inch	Ultimate Load: Average Pound Per Inch	Theoretical Stress at Failure: Average Shear on Wedge	Theoretical Stress at Failure: Maximum Tension Below Load	Theoretical Stress at Failure: Maximum Tension Along Edge
One Load at Center of Edge							
Failure by shear wedge and splitting							
1	14	40,000	10,000				
5	14	66,890	16,720				
9	14	60,000	15,000	13,900	1750(1)	190(4)	-
19	42	77,000	19,250				
27	42	46,800	11,700				
30	42	65,000	16,250	15,700	1950(1)	210(4)	-
10	84	37,000	9,250				
14	84	78,000	19,500				
18	84	72,000	18,000	15,600	1950(1)	210(4)	-
One Load 6 inches from Corner							
Failure by shear wedge and splitting or top tension							
1	84	76,700	19,200				
6	84	59,000	14,750				
16	84	54,900	13,720	15,900	1990(1)	-	-
One Load at Corner							
Failure by top tension and shear wedge							
3	14	23,550	5,890				
7	14	29,940	7,480				
15	14	26,650	6,660	6,640	1660(2)	-	<1160(3)
12	42	35,420	8,870				
15	42	28,800	7,200				
31	42	17,600	4,400	6,820	1700(2)	-	<1190(3)
3	84	28,000	7,000				
7	84	26,800	6,700				
12	84	24,000	6,000	6,570	1640(2)	-	<1150(3)
Two Loads 6 inches from Corner							
Failure by tension at center of slab							
11	14	32,970	8,240				
13	14	34,980	8,740				
17	14	24,060	6,020	7,660	-	-	450(5)
21	42	26,500	6,620				
24	42	29,100	7,280				
25	42	21,500	5,380	6,430	-	-	380(5)

(1) For edge load, based on Eq.(7-b) $s = b = 1.0$ inches $A = 37^\circ$, $u = 26\text{-}1/2^\circ$

(2) For corner load, based on Eq.(13) $c = 2$ inches, $\theta = 45^\circ$
also average shear on 45 degree plane from inner edge.

(3) For corner load. based on Eq.(14) $t = 1.0$ inches, $\theta_s = 45^\circ$ $r = 4$ inches
Absence of reactive forces prevents high tension stresses away from the load.

(4) For edge load. based on Bleich, $0.65\ p/L$

(5) For 2 corner loads, based on Eq.(14) $t = 6$ inches, $\theta_s = 45^\circ$ $r = 24$ inches

than the concrete modulus of rupture. The concrete tension strength would be a more accurate gage of cracking in deep flexural members. The cracking between the 2 loads gives ample evidence for high tension stress along the loaded edge where radial stress distribution can occur effectively from loads near corners.

CRITICAL STRAINS

Strains at appropriate observation points have been examined for further information on the modes of failure. Special attention has been given to radial and tangential strains below the center load in an effort to determine splitting tension failure; also to strains near corner loading to determine tension stresses near the loaded edge.

Observed strains varied over a wide range; however, average strains at a point from several slabs appear to give a representative value. It has been found in other tests that maximum strains in tension generally is limited to between 100 and 200 microin per inch higher observed strains indicate incipient or widening cracks or plastic deformations during the progress of adjustment to loads in the critical range.

Critical Strains for Edge Loading. Strains below the concentrated load at mid-section were observed on Slabs 5, 9, 19, and 14 to 60 kip or higher loads; ultimate loads were 60, 67, 77, and 78 kips, or average p_{ult} = 17,600 pounds per inch thickness. Figure 7 shows average rosette strains 3, 6, and 9 inches below the load center and 3 inches away on the 45° plane. The range of strains is indicated as well.

A general comparison between vertical and horizontal strains directly below the edge load is given in Table 2 for loads at which plastic readjustment probably did not predominate. (The 30 kip load equals 3,750 psi contact pressure, about equal to the cylinder strength.) All slabs with strain observations suitable for interpretations were averaged, including the immediate readings on time-loading slabs for 20,000 pound load; the values in Table 2 accordingly represent 6 to 15 slabs.

The horizontal (tangential) observed strains are part Poisson's ratio effect, part direct stress induced. They indicate tension on the mid-section at all loads for any reasonable assumption of the value of Poisson's ratio, 0.20 used in Table 2. For low loads the tension seems to be highest at 3 inch depth, but for increasing loads the maximum tension on the mid-section appears to be 6 to 9 inches down into the slab, and the tension strain at 3 inch depth decreases. The tension stress at 9 inch depth, assuming 4,000,000 psi modulus of elasticity, would be about 120 psi at 30 kip load.

TABLE 2 - VERTICAL AND HORIZONTAL OBSERVED STRAINS BELOW CENTER LOAD.

Load on 4 in edge kip	Rosette location below load inch	Strain, microin per inch			
		Radial		Tangential	
		Observed (vertical)	Poisson's ratio 0.20	Observed (horizontal)	Tension Strain
		e_x	μe_x	e_y	e_t
10	3	-90	-18	+ 38	21
	6	-55	-11	+ 20	10
	9	-35	- 7	+ 13	6
20	3	-218	-44	+ 65	22
	6	-100	-20	+ 40	21
	9	-69	-14	+ 37	24
30	3	-390	-78	+100	23
	6	-160	-32	+ 65	35
	9	-106	-21	+ 50	31

Note:

$$e_t = \frac{e_y + \mu e_x}{(1 - \mu^2)}$$

$$e_c = \frac{e_x + \mu e_y}{(1 - \mu^2)}$$

The graphs in Figure 7 show disproportionate increase in strains 3 inches below the edge at loads above 30 kip, but not 6 and 9 inches below the edge. The horizontal strain at 3 inch depth for the higher loads is a reversal of the trend indicated by Table 2; this is interpreted to indicate increasing plastic horizontal displacement at that depth for the higher loads, incident to shear wedge mode of failure.

Maximum strains to failure in tension indicated by flexural tests do not exceed 150 to 200 microin per inch. Higher horizontal strains, Poisson's ratio deducted, were observed at 3 inch depth for 50 kip and higher load. Maximum mid-section tension, indicated by Table 2 at 6 to 9 inch depth, is not accompanied by exceptionally high strains for 60 kip load according to the 6 and 9 inch strain graphs in Figure 7, 50 to 60 microin per inch when Poisson's ratio is deducted. Tension strains - and stresses- at 6 and 9 inch depth accordingly would have to increase abnormally near ultimate load. Splitting tension failure, accordingly, is a result of shear wedge forces as initial failure, increasingly noticeable 3 inches from the load on the 45° section as well as the mid-section, as shown in Figure 7.

Critical Strains for Corner Loading. Local failure under corner load occurs in accordance with predicted shear wedge stress. Critical strains have been examined for some indication of stress conditions causing the vertical crack inward from the distributed corner load.

Linear strains were observed on lines one inch from the top and side edge. Rosette strains nearest the distributed load were observed at the 45° plane about one inch inward from the distributed load and 2 inches below the top edge. The location of the strain gages, and graphs of the strains in relation to load are shown in Figure 8. In the linear strain graphs the average strain and the maximum and minimum strains are shown; in the graph for the rosette strains radial, tangential and diagonal strains and the extreme values are shown. Theoretical stresses at the observation points obtained from Figure 18 of Appendix A, are indicated on the sketch as well.

Referring to strain gages one inch below the top edge, for the highest load with several measurements 20 kip, the average strains were -0.00005, +0.00013, and +0.00010 at 4, 7, and 10 inches from the corner. Indicated prorated strains at failure for 6,700 pounds per inch thickness would be about -0.00007, +0.00017, and +0.00013. The tension strains 7 and 10 inches from the corner are in the critical range at failure, sufficient for tension cracks at the top edge some distance from the load, where however, no crack was observed.

The crack immediately at the inner end of the distributed load is in a region of predominant compressive stress; however, high tension stress occurs very near the load along the load edge. Radial and vertical compression strains predominated at the 45° rosette gage; as well as one inch below the top edge, 3 inches from the load center. Accordingly, shear appears to have been the primary cause. Once started, high tension stress concentration at the bottom of the crack would explain its continued progress downwardly away from the side edge, divergent from the local shear wedge failure.

STRESS DISTRIBUTION OBSERVATIONS AND THEORY

The following study of stress distribution is intended for comparison of actual stresses as deduced from observed strains at loads in a possible design range with stresses indicated by the various theories and elemental approximations. The study indicates service stresses at and between spaced prestressing cable end anchorages. It supplements the data on critical strains and stresses at ultimate loads, indicates limitations in these exploratory tests, and suggests further experimental investigations.

Stresses have been determined from observed strains, averaging the values from as many slabs as possible. So that abnormally high occasionally observed tension strains at incipient cracks much below failure loads might not influence the average inordinately, the approximate upper limit of tension strain 150 microin per inch has been used for appreciably higher observed tension strain values.

The data on stress distribution given below were obtained in the short-time tests from the strain changes during loading, and - for edge loadings - from strain readings shortly after loading in the long-time tests. Stress distribution is determined for 20,000 pound edge loads and for 16,000 pound corner load, sufficiently high to indicate consistent strain, but well below ultimate loads to avoid major plastic displacements. (Contact pressure for 20,000 pound load was 2,500 psi, well below the cylinder strength.)

In general, the highest strains were consistently observed at 42 day age; otherwise, no relation was evident between age and strains. The modulus of elasticity in compression for 14, 42, and 84 day age averaged 4.5 million psi (including 4.9 million at 42 days), with a higher value probable for low strains. The modulus of elasticity in tension may be somewhat lower than in compression, as indicated in correlated flexure tests. Theoretical stresses at the points of observation were generally less than 1,000 psi, for which higher values than the secant modulus

to 50 percent of ultimate strength should apply. Observed strains have been converted into stresses assuming 4.5 million psi modulus of elasticity for edge loadings, based on strains in long-time tests on slabs, all well over 100 days old at loading, as well as in the short-time tests, and 4.0 million psi for corner loading involving only short-time tests.

The comparison between theoretical stresses and those computed from strains, gives a direct judgment on the appropriate choice of modulus of elasticity. A too low value of assumed modulus would result in stresses consistently lower than actual at most or all points, and would also show consistently lower than theoretical stresses which are independent of any assumed modulus of elasticity. The different assumed modulus values for edge and corner loading are indicated by such comparisons.

For determination of principal stresses from observed strains Poisson's ratio of 0.20 has been assumed. Variations in this ratio influence especially the principal tension stresses in tangential direction to the predominating principal compression stresses. No value could be deduced from the tests themselves; somewhat higher than the usually assumed value of 0.15 is suggested by low experimental strains and two-directional stress distribution. A lower value of Poisson's ratio would result in higher tangential tension stresses deduced from the observed strains.

Stress Distribution Near Edge Loads. Figure 9 shows directions and values of the principal stresses computed from all rosette strains, and the stress corresponding to linear strains one inch below the top edge, near a 20,000 pound edge load (5,000 pounds per inch thickness). The theoretical compressive stresses, assuming simple radial distribution for the load distributed over 2 inch length, are shown within ( ) under the principal compressive stress. In the central 45° sector on each side of the load the direction of the principal compressive stress deduced from strains was in no case more than 7° and averaged only 3-1/2° deviation from the theoretical direction, according to Timoshenko(1).

The decrease in magnitude of principal compression with increasing depth, as well as principal stress direction, shows good agreement with the stresses based on simple radial distribution. At the mid-section, especially, the variation in experimental and theoretical stresses coincide closely. Away from the mid-section the principal compressive stresses appear to average slightly higher than the theoretical radial distribution, with gradual deviation toward horizontal direction at the 60° plane, with flexural stress due to the experimental slab support a possible influence.

Tangential tension stresses are indicated under the load consistently, maximum at 6 inch depth. In simple radial distribution no tangential tension stress would occur; zero tension could be deduced from the observed strains only for Poisson's ratio from 0.3 to 0.4. The experimental tension stress, Figure 9 and Table 2, of about 90 psi equals 0.9 x 20,000/4x48. Although the 36 inch deep 48 inch long slabs did not have the preferred H/L ratio for comparing theory and experiment, the observations in these limited exploratory tests indicate closer agreement with the higher Bleich and Dischinger stress values, Equation (4) than with the lower values suggested by Guyon.

Stress Distribution Near Corner Load. Figure 10 shows directions and values of the principal stresses computed from the rosette strains and linear strains one inch from the top and side edges near the 16,000 pound corner load (4,000 pound per inch thickness). Values of radial stresses based on Equation (14) for distributed load computations (Figure 18) are shown within ( ) under each principal stress. Strains at the 2 points on the plane 30° from the top edge were inconsistent and small, indicating approximately zero stress; the points are in the neutral region for corner force radial distribution.

Based on 4,000,000 psi modulus, the principal stresses and linear-strain stresses below the load are not in close agreement, indicating a modulus of elasticity considerably higher than assumed. In addition the load was apparently distributed away from the corner near the top edge, noticeable 3 inches away at the 45° strain rosette as a 600 psi nearly vertical principal stress at that point. The inward distribution of load is noticeable in the 200 psi compressive stress one inch below the top edge as well, where radial tension should be present. Further away, one inch below the top edge, tension stresses occur, but much lower than the radial stress indications 400 psi at 6, 360 psi at 9 inches from the load, compared to about 240 and 280 experimental stress. It is probable that some deformation of the test slab could occur toward the loaded corner, and that there was sufficient friction at the load point to direct the load inwardly, at the same time decreasing the tension stresses along the top edge, below values which would occur in a large slab.

Stress Distribution for Symmetrical Loads. Figure 11 shows principal stresses computed from rosette and linear gages one inch from the top and side edge near 20,000 pound loads, each applied 6 inches in from the corner of the 48 inch top edge, and stresses at center between the 2 loads. Theoretical stresses near the loads would be the same as shown in Figure 9. Stresses are computed for 4.5 million psi modulus of elasticity.

Typical radial stress distribution near loads 6 inches from a corner is confirmed by the observed strains. Near the load stress distribution is substantially equal toward the edge and toward the center. Compared to Figure 9, stresses directly under the load are slightly higher, those at 30° and 45° planes somewhat lower. Horizontal tension stresses 3, 6, and 9 inches under the load are substantially the same as in Figure 9, with maximum tension 110 psi at 9 inch depth. The high tension stresses on 30° planes 6 inches from the load are apparently caused by local adjustments. The high tension stress near the top edge on the slab center section is apparent, in excess of 300 psi at the top edge. Equation (14) would indicate for 2 loads stress at the top edge 290 psi one inch below the edge 270 psi, and 2 inches below the edge 240 psi, compared to 280 and 220 psi observed one and 2 inches down, respectively. Equation (14) gives representative stress values for this loading.

Tension stresses along an edge between spaced loads apparently can be critical. For constant total loads the edge stresses, 1.0 p/a according to Reference (3), would apparently be constant and independent of the magnitude of individual loads, but that theoretical relationship may not hold in practice, considering the high compressive stresses near the loads. Between spaced loadings against a continuous edge the edge stress according to theoretical studies, would be only slightly - if at all - lower than indicated by these tests for equal spacing. These edge stresses could be critical in design. Further experimental investigations to clarify these stress conditions are needed.

In the long-time tests the immediate strains one inch below the edge at center between symmetrical loads were much lower than those observed in the short-time tests, 20 compared to 60 microin per inch. In the long-time tests, the slabs were loaded with opposed concentrated forces, so that only 18 inch depth was available for radical stress distribution below each load, and stresses on the mid-depth section could not be assumed evenly distributed. The immediate strains 9 inches below symmetrical loads in the long-time tests averaged 37% higher than corresponding strains in the short-time tests. Stresses on sections away from the loads in the long-time test were not typical for deep-beam conditions.

LONG-TIME STRAIN CHANGES

The long-time tests included strain observations for 20,000 pound concentrated loads opposite each other across the 36 inch slab dimension, applied on 3 slabs for each of 2 load conditions:

A. Opposing loads at center of each 48 inch edge,

B. Opposing symmetrical loads 6 inches in from the 2 corners of the 48 inch edge.

Strain gages and rosettes were applied to one side of the slab only, but near both concentrated loads and in both quadrants. The slabs were resting on one 36 inch edge with free air circulating around. Because of effective depth of only 18 inches with the particular loading arrangement, as mentioned before, only strains near each load can be considered representative for two-dimensional stress distribution. Strains were observed immediately after loading, at 1, 3, 7, 15, and 30 hours and after 4, 8, 16, 32, and 50 days' duration.

Generally, the 6 to 12 immediate strain readings for one point in the long-time tests were fairly uniform and in good agreement with the corresponding average of the short-time tests for points near the load. The long-time strains became increasingly non-uniform with increasing age, many gages undergoing extreme elongations after about one month on the center loaded slabs, and in some cases as early as one week on the slabs with symmetrical loads.

On one slab under symmetrical loads, Slab 8, all gages show very substantial rapid and uniform shortening, averaging between 250 and 300 microin per inch at 8 days, and more at 50 days on most gages.

The excessive elongation trends on many gages during the latter period were in some cases a reversal of earlier shortening, in others a continued or increased rate of elongation, in any case quite different from the general and continuing shrinkage on Slab 8, on which a few gages also indicated a reversal after one month. Slab 8 readings undoubtedly were influenced by pronounced shrinkage near the loaded edges, or compensation gage change, and have been omitted from consideration. The excessive elongation development on many gages has been attributed to gage breakdown; such readings have been omitted when indicating a decided reversal of earlier shortening, or excessive elongation. All positive strain readings over 150 microin per inch have been omitted from average values.

Figure 12 for center loads, and Figure 13 for symmetrical loads, show the changes in strains near the load points to 50 day ages. For rosette gages, the radial, r, the tangential t, and the diagonal strains d, have all been shown in the same graphs. The graphs are placed in substantially the position of the points on the slabs, all with time after loading to 50 days as abscissa and strains (elongation positive) as ordinates.

Compression strains predominate, as would be expected near concentrated loads. Initial elongations along the top edge and tangential strains change to shortening after a few days at most. Shrinkage may have contributed; however, compression strains along the top edge would be expected for the centrally loaded slab evenly supported under its bottom edge. The shortening one inch down along the top edge, Figure 12, is greater 3 inches from the load than directly below the load. Consideration of the load 6 inches from the corner as an edge load, rather than corner load, is confirmed by fairly uniform distribution of strains in both directions near the load.

Substantial creep undoubtedly occurred in vertical direction below the loads, visible in both radial and diagonal strains on the load center lines. There are no clear indications of tension strains incident to this downward deformation for center load in Figure 12; however, Figure 13 indicates tension strains of some magnitude.

Under the loads 6 inches from the corners, tangential elongation increased sharply during the first week or 2, visible 3 inches below the loads, and more particularly at strain rosettes 45° on each side. These tangential strains from 60 to 100 microin per inch indicate tension stresses on the 45° radial planes on each side of the load, coincident with relatively low radial strains. Such diagonal tension stresses could precipitate radial cracking and decrease the resistance to local failure near concentrated loads. The long-time loads of 5,000 pounds per inch thickness are about 1/3 of the local failure loads in short-time tests, while the maximum tension strains on the 45° planes are roughly one half of ultimate tension strains from beam tests. The exploratory tests did not include loads to failure after long-time loading; however, the above data indicate the possibility of diagonal tension which might require consideration near concentrated edge loads.

TEST CORRELATIONS

The exploratory tests covered by this report included only the 2 inch length of rectangular bearing. End supports for prestressing cables might be of different shape and may not cover the full thickness of the slab. It is logical to expect that concrete resistance to local failure will be greater away from the face of the concrete than at the face of the concrete. The rectangular bearing extending across the edge from face to face would then give a conservatively low value of strength compared to a bearing of equal area not extending to the slab faces. The equivalent length of a circular bearing might be estimated, considering shear wedge width to be somewhat greater than that of the full thickness equal area rectangular bearing.

Published tests on round bars bearing in concrete blocks provide a measure of correlation of the tests on 2 inch bearings to other bearing dimensions. The tests were made at the Bureau of Standards and have been reported by H. Marcus(7). They included bar sizes from 3/4 to 2 inch diameter embedded with their axis even with the face of concrete blocks and subjected to evenly distributed line loads perpendicular to the concrete.

Referring to 2 inch bars, local failure resistance averaged 13,000 pounds per inch which compared to average 15,300 pounds per inch for the tests on flat bearings in this report, with concrete of about equal strength. The agreement is remarkably close; the slightly lower strength for round bars is not surprising, considering the greater concentration of bearing pressure and inclination to wedging action under round bars.

The tests on different bar diameters for blocks with $H/L \geq 1.0$, of concrete with 3,800 psi average cylinder strength, showed linear relation between failure strength and bar diameter d , with average load resistance, and ultimate bearing pressure on the diametric plane, as follows:

for d = 0.75 in.,	7,500 lb	per in. length,	10,000 psi bearing;
for d = 1.00 in.,	8,800 lb	per in. length,	8,800 psi bearing;
for d = 1.50 in.,	10,600 lb	per in. length,	7,100 psi bearing;
for d = 2.00 in.,	13,000 lb	per in. length,	6,500 psi bearing;

Local failure by radial cracks and/or splitting occurred in all the tests. The load resistance per inch of length increased with diameter very nearly at linear rate, expressed as (4,000 + 4,500 d) pounds. The resistance of 4,000 pounds per inch of bar length is interpreted as load spread outwardly on each side of the bearing, independent of bar size, dependent upon concrete structure. The expression indicates a contribution of the concrete, equivalent to 0.9 inch, or 0.45 inch one each side of the bar. The shear on critical shear planes with (d + 0.9) inch base and 80 degree apex angle would be stressed to 1.900 psi for all bar sizes, or $f'_c/2$.

These tests give support for the shear wedge stress computations to predict failure, and indicate that bearing loads are spread over a wider effective bearing through coarse concrete

---

(7) H. Marcus; Load Carrying Capacity of Dowels at Transverse Pavement Joints, Journal American Concrete Institure, Vol. 23, No. 2, p. 169 (Oct. 1951).

aggregate. Ultimate loads computed in accordance with Equation (8) would be conservative, especially so for small bearing dimensions.

DESIGN APPLICATIONS

These exploratory tests have given some indications to critical tension stresses which must be considered in design near and between force concentrations imposed by end anchorages of prestressing cables at the ends of pavement slabs. Design rules cannot be formulated on the limited range of variables in the exploratory series of tests; however, the test results agree sufficiently well with some theoretical considerations to make tentative predictions of critical design conditions concerning tension stresses on principal sections:

A. On the vertical sections in line with the prestressing cables some distance in from the edge,

B. Along the edge between end anchors,

C. On the diagonal radial planes on each side of end anchorages.

BEARING CAPACITY

The ultimate capacity in bearing p_{ult} per inch thickness, limited by shear wedge failure, for rectangular full depth bearing of dimension c along the edge, and concrete cylinder strength f'_c, can be estimated in accordance with Equation (8):

$$p_{ult} \sim 2.0\, f'_c \cdot c$$

In Prestressed Bridges[8], where the ends of the beams are usually not covered from side to side with bearing plates, the allowable bearing pressure f_c is inversely related to the ratio between the bearing plate area a_p, and the area a_c of that portion of the end of the beam which is geometrically similar and concentric to the area of the bearing plate, as follows:

$$f_c = 0.4\, f'_c \sqrt[3]{\frac{a_c}{a_p}}$$

---

(8) Criteria for Prestressed Concrete Bridges, Department of Commerce, Bureau of Public Roads, 1954.

The unit pressure cannot exceed f'_c. Considering the high safety margins normal for bridges, it would seem appropriate to use a somewhat higher bearing stress for the allowable bearing pressure under pavement end anchor plates. The suggested allowable bearing p_b per inch of thickness is:

$$p_b = 0.60\ f'_c \cdot c$$

Bearing plates at pavement ends would probably extend nearly from top to bottom of the slab edge. The safety factor for local failure would be over 3.0 for full-depth bearing plates, and the allowable bearing pressure up to 50 percent higher than allowed for bridges with similar bearing.

The tests did not include the normal field condition, with a part of the concrete sections perpendicular to the edge taken by cable tubes or holes prior to grouting and somewhat higher stresses for that reason. Such temporary stresses would result in lower safety factor for a limited early period, with some increase in strength probable after grouting, possibly to strength about equal to that without holes.

Considering the relatively high safety factor applied to bearing stresses, there is some assurance against serious tension stresses developing with time on the 45 degree planes on each side near the anchorages. Nevertheless, the possibility of such stresses exists and may require design consideration to avoid diagonal tension cracks.

TENSION STRESSES ON CABLE LINE SECTION

For the 2 inch bearing used in the tests, local shear wedge failure evidently preceded splitting. Bearing capacity is apparently increased in direct proportion to bearing length, without change in shear wedge stresses. Tension splitting stresses, on the other hand, increase in nearly linear proportion to bearing capacity, as they are relieved only slightly by increase in bearing length.

Maximum tension stress on the sections in line with the cables, spaced distances a apart according to this investigation should be anticipated to at least equal the values found by Bleich and Dischinger:

0.65 p/a for 0.05 a bearing length c, or c/a = 1/20
0.60 p/a for 0.10 a bearing length c, or c/a = 1/10

If anchorage bearing pressure is $p_b = 0.6\ f'_c\ c$, the maximum tension for that anchorage capacity and above bearing lengths would be $0.0195\ f'_c$ and $0.036\ f'_c$, respectively.

Tension reinforcement generally has to be provided in structural concrete design if computed concrete tension exceeds $0.03\ f'_c$. Tension reinforcement perpendicular to the prestressing cables should accordingly be required under bearings at full design pressure with dimension c over 0.08 of the cable spacing a. The tension stress of $0.03\ f'_c$ is much lower than flexural tension generally considered acceptable in pavements; however, additional load and restraint stresses occur as well. If the concrete section is permanently cut by prestressing tubes, the tension splitting stresses on the net section would be increased correspondingly. Splitting tension stresses should therefore be computed on the net section.

The total splitting tension to be provided for with reinforcement following Bleich's solution, would be:

for $0.05\ a$ bearing $0.29\ p$
for $0.10\ a$ bearing $0.27\ p$
for $0.20\ a$ bearing $0.23\ p$

The reinforcement should be centered near one-fourth of the cable spacing from the edge. Splitting tension stresses are highly localized horizontally; between the cables compression stresses would occur at distances in from the edge more than one-fifth of the cable spacing.

For design, a maximum tension of $0.036\ f'_c$ was indicated for a bearing $0.10\ a$. The prorated tension at ultimate load would be $0.108\ f'_c$. This is a critical stress and for bearing dimensions 10 percent or more of the cable spacing splitting stress could be more critical than bearing stress. The minimum splitting tension stresses suggested above were exceeded slightly for the loads shown in Figures 9 and 11, although that may have been due to the experimental slab dimensions. For ultimate load the splitting tension stresses were about twice those computed in Table 1. Tests with larger bearing dimensions would be necessary to establish whether or not higher values of tensions could become critical without prior shear wedge formation.

EDGE TENSION BETWEEN CABLE ANCHORS

The occurrence of critical edge tension stresses between 2 concentrated forces was demonstrated experimentally. The stress between several spaced forces was not investigated. Theoretical investigations indicate only relatively small decrease in stress between single and continuous spans. The maximum tension at the edge should be estimated to be equal to the evenly distributed prestress, $1.0q$.

Reinforcement to carry the tension stresses would generally be required for prestressing intensities anticipated to be

practical in concrete pavements. The tension would be concentrated near the edge decreasing to zero at one-fifth of the cable spacing in from the edge.

The total tension to be provided for would approximate $0.20\ a \cdot q/2$, or $0.10\ p$. The reinforcement should be centered $0.07\ a$ from the edge.

The total edge stress between end anchors is about one-third of the sum of splitting tension stresses; however, high edge tension stresses appear to be more critical in their visible effects. Conventional reinforcement would become effective only after cracking had occurred. Considering combinations of relatively high edge stresses with wheel load stresses, limited transverse prestressing near the slab ends may be warranted, perpendicular to the longitudinal prestressing cables. Such prestressing could be dimensioned to resist part of the splitting tension forces as well.

End Spacings. The edge tension stresses suggested to be considered above are those anticipated in deep beams without decrease for continuity. Accordingly, equal reinforcement should be adequate also inward from the prestressing anchors nearest the slab corner, provided the bearing is not so near the corner that edge tension stresses for corner load would need to be considered (within 10 c distance). Edge tension stresses rise to estimated magnitudes within a short distance on each side of the bearing. Edge reinforcement must accordingly be well anchored near the corner.

CORNER LIMITATIONS

Corner Bearing Capacity. The tests have shown that loads applied immediately adjacent to a corner are limited to failure at pressures equal to the concrete cylinder strength f'_c, rather than $2.0\ f'_c$. The allowable bearing pressures under end anchorage bearings extending to a corner should accordingly not be greater than $f'_c / 3$.

The tests show, further, that 2 inch bearings centered 6 inches from a corner have equal capacity to bearings far away from the corner. Accordingly, the bearing capacity for edge loads would be applicable to end anchors centered not less than 3 times the bearing dimension c from the corner.

Edge Tension Near Corner. For bearings near a corner the possibility of critical tension stresses for some distance inward from the bearing must be anticipated. The maximum tension along the top edge indicated in the corner tests is given by Equation (14), and could occur about $2\ c$ in from the corner. For a maximum capacity of a corner bearing of $f'_c \cdot c/3$, the equivalent maximum tension stress would be:

$$0.17\ p/t, \quad \text{or} \quad 0.34\ \frac{p}{c}, \quad \text{or} \quad 0.113\ f'_c$$

The tension along the edge is in the critical range for design values of bearing at the corner. Tension reinforcement would of necessity have to be provided near corners, or corner bearing plate dimensions increased greatly.

The edge tension near corners can be effectively decreased if the prestressing anchorage is placed a short distance away from the corner; centering the bearing plate at 2 c from the corner would decrease the critical edge tension to one-fourth of the value for corner bearing. Long-time load tests were not performed for corner load; it is possible that creep in compression along the loaded edge could increase the tension stresses along the bearing edge appreciably, leading to cracks of the orientation sometimes observed on conventional pavements at transverse joints restrained because of joint infiltration. Without additional tests, tension reinforcement along the bearing edge should be conservatively dimensioned.

Total tension to be resisted by reinforcement along the bearing edge may be dimensioned on assumed radial stress distribution for concentrated corner load as outlined in Appedix A, adjusted for the dimensional variations due to load inward from the corner. For a single concentrated load at the corner, the resultant tension force is 0.4 P , Figure 17. For a load some distance in from the corner it decreases to less than 0.2 P at the section of maximum stress, but increases in total amount with increasing distance along the loaded edge, toward the 0.4 P value, although with greatly decreased stress intensity. The stress values and total force for corner loads are valid only between the corner load and the next load against the edge.

In relation to a total corner bearing force p of f'_c c/3 , radial distribution stress of 1.36 p/r would be not over 0.03 f_c at 15 c distance from the corner. The tension reinforcement would not be theoretically required beyond that distance from the corner; considering actual lower stresses probably not beyond 10 c distance from the bearing. The corner bearing tension edge reinforcement is about 3 times that required between spaced edge anchors. For spaces between bearings the center portion of which extend to less than 10 c distance from a corner, it is prudent to increase the edge reinforcement above that required between spaced edge bearings. The reinforcement must be anchored at the corner to be fully effective a short distance away.

CONCLUSIONS

The investigation was undertaken to explore experimentally the pertinent force and stress concentrations near prestressed pavement ends, because no prior tests were known concerning the effects of widely spaced concentrated edge loadings against slabs under substantially 2 dimensional stress distribution. Critical stress conditions were discovered, but no attempt was made to cover dimensional and material variables. Conclusions based on this exploratory investigation are tentative and are in part based on theoretical studies, which were supported by the test results, and on correlation with the round bar tests.

Considering the exploratory nature of the investigation, the scope of information obtained from the tests was unusually wide and inclusive.

1. The 4 inch thick 48 inch wide and 36 inch deep slabs loaded vertically through a 2 by 4 inch steel bearing plate against the 4 inch edge were adequate for observation of stress distribution near the loads.

2. Stresses near edge loads were in good agreement with predictions based on simple radial distribution for loads centered 6 inches or more from a corner, except as to observed tension strains on the load-line section in the experiments.

3. Edge and corner loaded slabs under the 2 inch bearing failed generally by crushing - "shear wedge failure" -. The ultimate bearing strength could be computed assuming shear failure on the sides of a wedge with the bearing plate as base, with bearing strength direct proportionate to length of bearing.

4. The shear wedge failure was followed by splitting failure in all tests. Tension strains were observed on the load line section although not of critical indicated magnitude prior to plastic adjustments in the formation of the shear wedge.

   The observed maximum tension strains were in substantial agreement with stresses computed in deep beams on sections of spaced force concentrations. The tension strains increased disproportionately near shear wedge failure. Critical splitting tension, without evidence of crushing, may govern in design for bearing lengths approaching and exceeding one-tenth of the spacing of the bearings.

5. Tension failure occurred near the center section between 2 symmetrical loads long before critical bearing stresses were reached. The tension stress equaled or exceeded that predicted for deep beams at center span between concentrated reactions.

6. Under lasting load substantial creep in compression was observed directly below the bearing. As a result tension strains on radial 45 degree planes on each side increased appreciably. Increased tension strains (diagonal tension) cannot be disregarded in design.

7. Cracking at failure under corner loading simulated closely so-called restraint cracks, frequently observed at transverse contraction and expansion joints of conventional concrete pavements.

8. Based on this experimental investigation, other cited correlated tests, and the theoretical studies, tentative criteria have been suggested as included in the chapter Design Application, for design of ends of prestressed pavements with spaced prestressing cable end anchors.

ACKNOWLEDGEMENT

The investigation covered by this report is part of a cooperative research project between the U. S. Bureau of Public Roads, the Missouri State Highway Commission, and the University of Missouri at its School of Mines and Metallurgy, Rolla, Missouri, to study the effects of prestressing upon thin concrete pavement slabs and the properties of concrete pertinent to such slabs.

General direction of the work from its inception in the highway department through planning, execution, and interpretation, has been the responsibility of F. V. Reagel, Engineer of Materials, Missouri State Highway Department. E. W. Carlton, Professor and Head, Department of Civil Engineering, Missouri School of Mines, Rolla, Missouri, directed and supervised the the investigation for the University of Missouri, including faculty supervision of the 2 theses for degrees of M.S., from which the experimental data in this report are taken. The investigations, data compilation, and theses reports were made by W. M. Baldwin for short-time tests to failure, and by J. B. Roberts for long-time tests and their interpretation.

For the Missouri Highway Department, E. O. Axon supervised material selection and proportioning, and construction of the slabs. Bengt F. Friberg, Consulting Engineer, St. Louis, was engaged for test planning, and for combination and condensation

of the research data in this report, including review of theoretical studies and the published tests, covered in Appendixes and the report, as well as extension of the theoretical studies to conditions of the tests, and design applications.

APPENDIX "A"

THEORETICAL STRESS DISTRIBUTION FOR EDGE FORCES

REFERENCE

The following information on stress distribution for forces against an edge and in the plane of a thin plate extending an infinite distance from 2 edges, acting either against the edge or at the corner, is taken from "Theory of Elasticity" by S. Timoshenko (McGraw-Hill Book Company, Inc. 1934), (1).

POINT LOADING AGAINST AN EDGE

Radial Stresses. The stress distribution in a vertical plate loaded at a horizontal boundary far from a corner with a vertical force on a line across the boundary, p per unit of thickness, is called simple radial stress distribution. An element on a radius r and angle θ with the direction of the force, Figure 14, is subject to a principal stress f_r directed toward the force application point, a radial stress of magnitude:

$$f_r = - \frac{2p}{\pi} \frac{\cos \theta}{r} \quad ; \qquad (1)$$

The tangential stress f_t is zero. The maximum shear stress v_r is on planes at 45° angle with the radius, and has the magnitude

$$v_r = \frac{p}{\pi} \frac{\cos \theta}{r} \qquad (2)$$

There is no shear stress in the radial and tangential planes of principal stress. On the symmetri section through the load, called the midsection, there is accordingly no normal stress and no shear stress.

As seen in Figure 14, $r/\cos \theta$ equals the diameter d of the circle through the load with the element on its circumference. The principal stress of all elements on that circle is therefore constant:

$$f_r = \frac{2p}{\pi \cdot d}$$

As there are no stresses on the midsection, the resultant of stresses on each side of the midsection can be obtained directly from the radial distribution stress. The sum of vertical components of stress equals p/2 on each side of the load point. The sum of the horizontal components of stress is obtained through integration:

Horizontal Force =

$$= \int_0^{\pi/2} f_r \cdot dA \cdot \sin\theta = \int_0^{\pi/2} \frac{2p\cos\theta}{\pi \cdot r} \cdot \sin\theta \cdot r \cdot d\theta;$$

$$= \int_0^{\pi/2} \frac{2p}{\pi} \cos\theta \sin\theta \, d\theta \, .$$

$$= p/\pi \, .$$

The integral, as seen, is independent of r ; the resultant force accordingly applies to any section between the midsection ($\theta = o$) and the top surface ($\theta = \pi/2$).

The resultant component forces on any section through the 90 degree angle on each side of the load, as shown above, are a vertical force $p/2$ and a horizontal force p/π . The resultant makes an angle of 32-1/2 degrees ($\tan\theta = 2/\pi$) with the direction of loading, and equals .59 p. (p/2 cos. 32-1/2). It can be taken as the equivalent of the force when considering sections in each quadrant.

The maximum shear stress at points on the circle circumference is constant as well, and acts on planes making 45 degree angles with the radius. These planes all go through points L and R on the circle, one radius to the left and to the right of the midsection. The loci of points L and R for all circles lie on two 45 degree lines through the load point. Critical shears could accordingly occur some distance out from the load point.

Vertical and Horizontal Stresses. The normal stresses on horizontal planes, f_x , and vertical planes, f_y , and shear stress on horizontal and vertical planes, v_{xy} , at a distance a below the loaded edge, Figure 14, are obtained directly from the radial stresses at different values of θ :

$$f_x = -\frac{2p}{\pi a}\cos^4\theta \qquad (3)$$

$$f_y = -\frac{2p}{\pi a}\sin^2\theta\cos^2\theta \qquad (4)$$

$$v_{xy} = -\frac{2p}{\pi a}\sin\theta\cos^3\theta \qquad (5)$$

Figure 15 shows the radial, vertical, and horizontal stresses, as well as shear stress, v_{xy} , at varying distances from the midsection. Directly under p there is only the vertical principal

stress, with no horizontal stress, or shear stress on the horizontal and vertical planes; but there is a maximum shear stress on the 45 degree planes equal to one half of the principal stress.

DISTRIBUTED LOAD

The coordinate stress values f_x , f_y , and v_{xy} , Equations (3), (4), (5), and Figure 15 can be used as influence values of stress for a distributed load. If, on a body of unit thickness, a force p perpendicular to the boundary is distributed over a length 2b , the intensity of load p/2b is the upper limit of vertical stress. For distributed load the midsection is not free from normal stress, but there is no shear stress on the midsection.

Figure 16 shows stress conditions for a distributed force. In the separate detail diagrams, related to depth below the boundary in units of b , are shown:

A. Vertical stress directly below the load center, as well as directly below the end of the loaded length, and , for comparison, stresses for equal point force (dashed lines) at the center of loading;

B. Horizontal stress on the midsection, and on the vertical section at distance b from midsection;

C. Shear stress on the vertical section at distance b from the midsection.

For a distributed force, the principal stresses are constant for all points on a circle with its center on the midsection and the loaded length 2b as a chord. The principal stresses are directed toward the intersections of the circle with the midsection as shown in Figure 16. All points on the circle have the same peripheral angle C for the loaded length as chord, and the 2 principal stresses f_a and f_b are:

$$f_a = \frac{p}{2b\pi} (C + \sin C) ;$$

and

$$f_b = \frac{p}{2b\pi} (C - \sin C) .$$

The vertical and horizontal compressive stress directly below the center of load are given below, also vertical stress relation to stress for equal point force:

	Vertical stress	Horizontal stress	Vertical stress/ conc. force stress:
at depth 0 ,	.5 p/b,	.5 p/b,	---
at depth b ,	.41 p/b,	.09 p/b,	64%
at depth 2b,	.28 p/b,	.02 p/b,	86%
at depth 3b,	.20 p/b,	.01 p/b,	93%
at depth 6b,	.10 p/b,	-- ,	98%
at depth 9b,	.07 p/b,	-- ,	99%

For depth of 2b or more there is no significant difference between stresses for distributed load and point force.

Immediately below the distributed load both vertical and horizontal stresses are p/2b . At the end of the loaded length the vertical stress at the surface changes from p/2b to zero; and the horizontal stress is p/4b , which also approximates the vertical stress a short distance below the top surface.

The direction of the resultant force in each quadrant is shown in Figure 16. The direction is vertical and magnitude p/2 at the top surface, but substantially the same as for point force at 2b depth. (The horizontal compressive stresses on the midsection near the load turn the resultant force from vertical toward 32-1/2 degree inclination with increasing depth.)

CRITICAL STRESSES FOR EDGE FORCE

Under load conditions of simple radial stress distribution, only compression and shear stresses exist in a semi-infinite isotropic material. Failure would be the result of critical shear stresses, and is not governed by axial compression values obtained from the unconfined cylinder strength tests.

In the concrete test cylinder, failure in shear is initiated along planes at 45 degree angle with the axial compression, at ultimate shear stress of $f_c'/2$, f_c' being the corresponding cylinder compression stress. For the edge forces, shear failure is localized near the load and generally referred to as shear wedge failure, the result of local concentration of shear stresses; however, the maximum shear stresses do not occur on plane 45 degree surfaces, and the shear stresses are relieved by plastic redistribution on the critical planes, confined in the surrounding concrete, so that maximum vertical loads have only indirect relation to the cylinder strength.

The location of critical shear planes is dependent upon load distribution, and, because failure can be initiated some short distance below the load, also on concrete composition, hard

coarse aggregate close to the load acting to distribute the load downward and outward from its concentrated application, with failure along weaker shear surfaces further away.

Critical Shear Planes. The following prognostication of failure for edge loading is developed from conditions relating to radial stress distribution. Inasmuch as there is no shear stress on the midsection, in simple radial stress distribution each quadrant can be analyzed separately in estimating initial failure conditions. It will be assumed that initial failure is the result of ultimate shear extending over a plane shear surface between the top boundary and the midsection on each side.

Point Force. In each quadrant a vertical force component $p/2$ and a horizontal force component p/π are the only forces which act on any section. (There is no normal force on the midsection.) The resultant force $.59p$ at 32-1/2 degree angle with the midsection is the only force on the sloping plane at an angle u with the midsection and intersecting the top surface at a distance s from the force. The shear force is $.59p \cos (32\text{-}1/2 + u)$, and the area of the shear plane $s/\sin u$, the shear v then is:

$$v = .59 \frac{p}{s} \cos (32\text{-}1/2 + u) \sin u.$$

The angle u for which the shear is a maximum is found by derivation, at zero value of first derivative:

$$\frac{dv}{du} = \frac{.59p}{s} \left\{ \cos(32\text{-}1/2 + u) \cos u - \sin u \sin (32\text{-}1/2 + u) \right\} = 0$$

from which, for maximum average shear:

$$u = \frac{90 - 32\text{-}1/2}{2} = 28\text{-}3/4 \text{ degree}$$

The average shear on this weakest plane would be:

$$v = \frac{.59p}{s} \sin^2 28\text{-}3/4 = .14\, p/s .$$

If the average ultimate shear v is taken as $f_c'/2$ this equation gives the ultimate load p_{ult} in terms of f_c':

$$p_{ult} = \frac{f_c' \cdot s}{2 \cdot .14} = 3.6\, f_c' \cdot s . \qquad (6)$$

If the resultant in each quadrant should be directed at some other angle A than 32-1/2 degree, its magnitude would be p/2 cos A . The shear stress would be:

$$v = \frac{p}{2s} \quad \frac{\cos(A + u) \sin u}{\cos A} \quad ;$$

and the angle u for maximum average shear stress:

$$u = \frac{90-A}{2} \quad ; \qquad (7\text{-a})$$

and the maximum average shear stress:

$$v = \frac{p \tan u}{4 s} = \frac{p \tan\left(\frac{90-A}{2}\right)}{4 s} \qquad (7\text{-b})$$

For concentrated line force across the edge the dimension s would be dependent upon plastic deformation directly at the force and upon hard coarse aggregate near the boundary distributing the force over some effective equivalent length 2 s .

Distributed Load. The same equations used to determine the angle of planes for maximum average shear are valid also for distributed load. The dimension 2s would equal the length 2b over which the load is uniformly distributed, perhaps with some addition for load spread through adjacent hard and strong coarse concrete aggregate. The direction of force in each quadrant is not constant as for point load; at the boundary it is vertical, and compression stresses on the midsection change its direction with increasing depth toward the 32-1/2 degree inclination. From the end of the loaded length maximum average shear would be on a plane making about 33 degree angle with the midsection, the resultant force on which plane is inclined about 24 degrees from the vertical (Equation 7-a), and the maximum average shear would be .16 p/s , somewhat higher than computed for point load. Within the shear wedge increasing plastic deformations take place under the high bearing pressures as failure is approached. Horizontal compression is correspondingly increased above theoretical values, so that the resultant in each quadrant near failure could be at much greater inclination than 24 degrees above the depth of the shear wedge, with the plane for average maximum shear, possibly even steeper than the 28-3/4 degree angle. Tension stresses on the midsection below the shear wedge would act to redirect the resultant toward the 32-1/2 degree inclination at greater depths. Equation (6) would probably indicate failure loads too low, rather than too high,

considering the above influences. For distributed loads over a short length $2b$, the following prognostication for ultimate load is given:

$$p_{ult} = 4\ b\ f'_c = 2c\ f'_c \qquad (8)$$

The above study is not intended to arrive at accurate values for design, but to explain the feasibility of seeminly high bearing pressures, and to give a basis for appraisal of local failures in the tests.

STRESS DISTRIBUTION FOR CORNER LOAD

Simple radial stress distribution applies to forces at the apex of a wedge shaped large body as well.

Point Force. Figure 17 shows the force in line with the bisector of a wedge with 2α contained angle. For this "axial" force P_s the principal radial stress f_{sr}, at angle θ_s with the direction of force, assuming a body one unit thick, is:

$$f_{sr} = - \frac{P_s \cos \theta_s}{r\ (\alpha + 1/2 \sin\ 2\alpha)} \qquad (9)$$

For a "transverse" force P_t, according to Figure 17, the principal radial stress, f_{tr}, at angle θ_t with the direction of force, is:

$$f_{tr} = - \frac{P_t \cos \theta_t}{r\ (\alpha - 1/2 \sin\ 2\alpha)} \qquad (10)$$

The tangential principal stress and shear stress on radial and tangential planes, are zero. The angles θ_t and θ_s are related as:

$$\theta_t = 90 + \theta_s$$

Equation (10) then takes the form:

$$f_{tr} = + \frac{P_t \sin \theta_s}{r\ (\alpha - 1/2 \sin\ 2\alpha)} \qquad (11)$$

Point Force in Line with Edge. By combining Equations (9) and (11) radial stress distribution for an apex force of any direction can be obtained. With reference to pavements, it is especially desired to determine stresses for force along one of the sides of a 90 degree corner. Force P along one side equals $P/\sqrt{2}$ in axial and transverse direction, each. The combined radial stress f_r would be:

$$f_r = -\frac{P}{r \cdot \sqrt{2}} \left(\frac{\cos \theta_s}{\alpha + 1/2 \sin 2\alpha} - \frac{\sin \theta_s}{\alpha - 1/2 \sin 2\alpha} \right)$$

For the 90 degree corner ($\alpha = \frac{\pi}{4}$) this equation takes the form

$$f_r = \frac{P}{r} \left(2.47 \sin \theta_s - .55 \cos \theta_s \right) \qquad (12)$$

As θ varies from $-45°$ to $+45°$, the radial stress varies from $-2.14\ P/r$ to $+1.36\ P/r$.

The radial stress distribution for a corner point force is shown in Figure 17. Zero radial stress is at an angle of 1.0 radian with the edge along which the force acts, or 32-1/2 degree below the top edge. The resultants of the compressive stresses approximate 1.2 P at an angle of about 20 degrees with the same edge. The resultant of the tension forces is about .40 P at an angle of 10 degrees with the other side of the corner. On circular sections with the corner as centrum the variation of the radial forces is nearly linear.

DISTRIBUTED LOAD AT CORNER

The following reasoning applies to load uniformly distributed over a short length from a corner inward along one edge and in direction parallel with the other edge. The stress distribution for corner point load is approached for sections far from the corner; near the load stress distribution is some combination of that for corner load and edge load.

Directly under the distributed load, the radial stress f_r, the tangential stress f_t and the radial-tangential shear stress v_{rt} are given by Timoshenko (loc. cit p. 122). For radius r ($r \leq c$) at angle θ with the loaded edge of a 90 degree corner, the stresses are:

$$f_r = -\frac{P}{2c}\,(1 - \cos 2\theta)$$

$$f_t = -\frac{P}{2c}\,(1 + \cos 2\theta) \qquad (13)$$

$$v_{rt} = -\frac{P}{2c}\,\sin 2\theta$$

It is seen that these stresses are independent of r ; the tangential (or vertical) stress at the loaded edge, and the radial stress at the side edge ($\theta = 0$ and 90 degree) both equal $-P/c$. The horizontal stress at the loaded edge is zero. The maximum shear stress is at the 45 degree diagonal and equals $0.5\ P/c$. There are no tension stresses in this region of the corner; the principal stress is vertical and equals $-P/c$.

Radial stresses on circular sections at greater distances from the corner than the loaded length can be appraised from the stresses for corner load. The force along the bisector P_s can be considered equivalent to an axial force, and the transverse force P_t equivalent to bending on the circular cross section of unit width. (The radial stresses for load P_t according to Equation (11) vary nearly linearly on the circular section, between plus and minus $P_t/\sqrt{2}\ (\pi/4 - 1/2)$ at the top and side edges, respectively.) The length of the circular section is $r\pi/2$; the moment of load P_t , considered as pure bending should equal the edge stress multiplied by the section modulus of the cross section $(r\pi/2)^2/6$, or

$$M = \frac{P_t \qquad (r\,\pi/2)^2}{\sqrt{2}\ (\pi/4 - 1/2)\ 6} = P_t\ 1.02\ r \sim P_t r$$

Stresses on the circular cross section accordingly, correspond closely to those for pure bending. The small difference of 2 percent is due to the stresses on the circular cross section between the edges and the bisector being slightly greater than linear variation assumptions.

A load P perpendicular against one side of a 90 degree corner, and applied at a distance t in from the corner, can be considered applied at the bisector at a distance $t\sqrt{2}$ from the corner with axial and transverse components each $P/\sqrt{2}$. The stresses of the axial component are represented by Equation (9); (for circular sections close to the load the radial stresses near the load would be somewhat greater, and the compressive stresses at the edges somewhat lower than Equation (9) values).

The radial stresses due to the transverse component would be proportionate to the stresses for corner load, Equation (11), decreased by the ratio of the lesser moment arm, $(r - 6\sqrt{2})$ for the bisector and $(r - 2t)$ at the edges of the circular cross section at radius r ; (although the moment arm is smaller near the 2 edges, the direct stress would increase on the circular cross section near the edges).

Considering the different influences, the stresses due to the transverse load $P/\sqrt{2}$, indicated by Equation (11), are considered decreased in proportion to $(r - 1.5\ t) / r$. The radial stresses on the circular cross section, combining Equations (9) and (11), then are:

$$f_r = \frac{P}{\sqrt{2}\ r}\left(\frac{-\cos \theta_s}{(\pi/4 + 1/2)} - \frac{(r - 1.5t)\ \sin \theta_s}{r\ \ (\pi/4 - 1/2)}\right)$$

or

$$f_r = \frac{P}{r}\left(\frac{(r - 1.5t)\ \sin \theta_s}{r\ \ 0.404} - \frac{\cos \theta_s}{1.82}\right) \qquad (14)$$

Radial stresses on various circular sections in accordance with Equation (14) are illustrated in Figure 18, which shows also locations of zero stress. At near $2t$ distance from the corner the top edge stress would be zero, and reach a maximum of $0.17\ P/t$ at about $4t$ distance from the corner. The neutral axis for radial stresses lies above the 32-1/2 degree sloping line which it approaches with increasing radius. Figure 18 shows the stresses at increasing distance from the corner compression along the side edge, and tension along the loaded edge.

For distributed loads the stresses in Figure 18 may be used as influence diagram. For short loaded length the stresses can be taken for load P concentrated $c/2$ from the corner.

Critical Stresses Near Distributed Corner Loads. The shear on the 45 degree corner sections directly below the load is $0.5\ P/c$. For vertical force resultant the 45 degree section would be subject to maximum average shear in accordance with Equation (7-b).

Shear Wedge. There is no horizontal stress at the side edge to influence shear stress. Failure would occur when the shear reaches $f'_c/2$ stress. Critical load for shear wedge failure at the corner would accordingly be for failure within the corner 45 degree plane:

$$P_{ult} = f'_c \cdot c \qquad (15)$$

Top Tension. The tension along the loaded edge for $c = 2t$ could reach $.34\ P/c$ maximum at a distance of $2c$ from the corner, as shown in Figure 18. For crushing load, Equation (15), the tension along the top edge would reach $0.35\ f'_c$ much above normal ultimate tension strength. Tension cracks would occur for high loads; however, the result of cracks perpendicular to the top edge would be to relieve the tension stresses immediately adjacent to the top edge without decreasing the load capacity, as long as the distributed load could be supported by the strip of concrete along the edge as a column.

The top tension stresses for distributed load are much lower than those deduced for concentrated corner force, shown by dashed lines in the appropriate stress diagram of Figure 18. In accordance with Equations (13) the stress along the top edge under a distributed corner load is zero. Using Equation (14) and Figure 18 as influence diagram to determine top edge stress for a distributed corner load, the tension stress along the top edge is found to equal the maximum stress immediately beyond the end of the distributed load and to remain nearly constant at $0.34\ P/c$ to $2c$ distance from the corner.

APPENDIX "B"

STRESSES ON AND BETWEEN LOADED SECTIONS AGAINST AN EDGE

STRESSES FOR DEEP BEAMS

For beams with depth large in relation to the span, elemental assumptions of plane stress and strain variation do not apply. For depth H not over one half of the span L elemental beam assumptions are considered sufficiently accurate. For greater beam depth flexural tension stresses near mid-span, and compression stresses at the supports, are concentrated over a decreasing portion of the depth, with approximately triangular distribution. The distance from the extreme fiber to the neutral axis at mid-span quickly approaches a constant value in relation to span; at the supports it varies somewhat with the width of support. There is substantially no change in stress for increasing depth to span ratios over 1.0.

A slab with concentrated loads against an edge can be considered as an infinitely deep beam, with the concentrated loads as reactions to the evenly distributed pressure on the slab section some distance from the edge. The spacing of the concentrated loads equals the span. Considering stress distribution in Equation (3) of Appendix A, the variation in stress on the section at distance from the edge equal to the spacing is less than 2 percent up or down from uniform stress.

Continuous Spans. Stress distribution in deep beams has been analyzed by Dischinger[2] according to the elastic theory. The results have been presented in English by the Portland Cement Association[3] for beams with depth to span ratio 1/2, 2/3, 1, and 00, uniformly loaded near the lower boundary and with reactions uniformly distributed over a length C of 1/20, 1/10, 1/5, and 1/2 of the span dimension. In Figure 19 stress distributions on the mid-span section, and on the mid-support sections are shown, with vertical dimensions given in units of span. Loads are considered per unit of span and thickness, q .

At mid-span, tension at the bottom is found to equal about 1.0 q , with nearly linear decrease to zero stress at a distance of 0.20 L above the bottom for beams of large depth. The total force in the tensile stress portion of the mid-span section is nearly 0.10 q L . In reference (3) stresses have been shown for loading and reactions both at the bottom of the beam and loading on the clear span only. For loading, other than near the bottom edge mid-span bottom tension and location of zero stress are not changed materially from Figure 19 values. Stresses on the support mid-sections must be increased proportionally for

full-span above clear span loading. As seen in Figure 19 there is no significant change in critical stresses and location of zero stress for H/L ratios over 2/3, when vertical dimensions are measured in units of span, for continuous spans loaded near bottom.

The stresses on sections through the center of support are of special interest for splitting stresses on sections in line with loads. The compressive stress at the bottom edge for reaction of q · L are 5 q, 10 q, and 20 q for support lengths of 0.20 L , 0.10 L , and 0.05 L , respectively. That horizontal compression equals the unit pressure of reaction, and also the horizontal stress at the contact surface for simple radial stress distribution of a distributed load as given in Appendix A. The compressive stress (Reference 3) decreases to zero at a distance of 1.1 b , 1.5 b and 2.0 b above the support of total length 2 b , extending horizontally b equal to 0.10 L , 0.05 L , and 0.025 L on each side of the section. Tension stresses reach maxima of 0.5 q , 0.6 q , and 0.65 q at distances of 0.25 L , 0.10 L , 0.15 L or 2.5 b , 3.5 b , and 6 b above the support for the 3 support widths, respectively. The stress decreases to near zero at a distance equal to L above the support, with no noticeable stress beyond in deeper beams. The total force on the tensile stress portion of the midsection over the supports is between 0.21 q L and 0.24 q L for the 3 support dimensions.

Single Spans. In Reference (3) stresses at mid-span have been developed for single as well as continuous spans, giving the following for bottom tension stress and location of zero stress above bottom for single spans:

	H/L RATIO		
	1.0	1-1/3	2
Edge stress	1.2 q	1.05 q	.95 q
Zero stress, up	.37 H	.27 H	.18 H
or	.37 L	.36 L	.36 L

For continuous spans with H/L equal to 1.0 or over the stress is 1.0 q and zero stress at 0.20 L above the bottom. Although, accordingly, there is no substantial increase in bottom edge tension stress for single spans in the deep beams, there is appreciable increase in tension portion of the section in single spans over continuous spans.

STRESS STUDIES FOR END BLOCKS OF PRESTRESSED STRUCTURAL MEMBERS

Transverse stresses below and between prestressing cable anchorages in the end blocks of structural members have been

analyzed, using graphical analogies of plane force trajectories. The unit forces are assumed parallel at the bearing plate, with their trajectories spread in double curved lines to even and parallel distribution on the cross section at a distance from the end equal to the depth or width of the member or the spacing of the anchorages. If the bearing dimension is c and the section dimension - or anchorage spacing - a, the forces at the bearing p/c spaced one unit apart would be spaced apart a/c at a distance of a. The general equation between the transverse stress $d f_y$ curving the force trajectories out of line y in distance x would be

$$d f_y = \frac{p}{c} \frac{d^2 y}{dx^2} \tag{16}$$

or for total force, from center of application y:

$$f_y = p \frac{d^2 y}{dx^2} \tag{17}$$

The force trajectories curve away from the center of bearing over a short distance below the bearing to inflection points on the curves, forced out by transverse compression stresses under the bearing, to a lesser extent, also by transverse tension stresses on each side of the bearing. Beyond the inflection points the force trajectories reverse curvature toward parallel and even distribution on the cross section, and in that greater distance, away from the edge, the changes in direction are forced by tension stresses on sections near the lines of load concentrations and compression stresses in the space further away on each side, and between parallel loads.

The end block stresses in prestressed members have been studied extensively by Guyon[4] both theoretically and with photoelastic methods. Guyon found the transverse splitting tension stresses (in end blocks called bursting stresses) for unit thickness to be distributed substantially as shown in Figure 20a for different ratios of bearing $2b = c$ and spacing a. The maximum bursting stresses in Figure 20a are somewhat lower than the maximum stresses in Figure 19 on the deep-beam midsection at centers of spaced supports of different lengths; those stress values and their locations have been indicated in Figure 20a as well.

A rigorous mathematical solution for the two-dimensional stress distribution in a plane of limited width under a concentrated distributed load was developed by F. Bleich[5].

Computations of the cumbersome solutions, applied to the stresses on sections on the load center line, have been given by S. Ban, H. Muguruma, and Z. Ogaki[6]. Figure 20b shows the distribution of tension stresses on the mid-section in accordance with Bleich's solution. Those maximum stresses are substantially higher than shown in Figure 20a, and very nearly the same as shown in Figure 19 on sections over supports in continuous spans.

Single and Continuous Spans. On sections in line with the loads as shown in Figure 20, mid-section maximum tension stresses for spaced loads, as studied by Guyon, are from 20 to 30 percent lower than the tension stresses for a single load according to Bleich. Stresses on mid-sections over spaced supports, as developed by Dischinger, are in much closer agreement with Bleich than with Guyon maximum stresses.

At a depth equal to the effective width of load distribution, a , the tension stresses on the mid-section shown in Figure 20 are insignificant. Reinforcement for the higher tension stresses nearer to the edge would normally be dimensioned for the total of transverse tension stresses on the section, for which the value integrated from Guyon's stresses, Figure 20a, does not differ greatly from the Bleich solutions. Comparative values of the total transverse force, per unit thickness, including also values derived from integration of the tension areas at support mid-sections in Figure 19 are as follows:

	Guyon:	Bleich:	Figure 19
bearing width 0	0.30 p	0.30 p	----
bearing width 0.05 a	0.26 p	0.29 p	0.24 p
bearing width 0.10 a	0.23 p	0.27 p	0.22 p
bearing width 0.20 a	0.20 p	0.23 p	0.21 p
bearing width 0.30 a	0.17 p	0.20 p	----

Tension Stresses between Two Loads. Tension stresses at an edge, the end of a prestressed member between 2 spaced anchorages, have been studied by Guyon, based on force trajectory considerations. Edge tension stress f_t between 2 symmetrical concentrated loads on an edge of length L , each L/8 in from the nearest corner, were found to equal:

$$f_t = 1.25\, q \qquad (18)$$

He found zero stress to be at a distance of 0.15 L away from the loaded edge. In Guyon's investigations it was assumed that the pressure q was evenly distributed at H = L . The value is considerably higher than found by Dischinger for continuous spans and deep single spans.

Stresses between 2 loads near the corners of an edge of length L can be computed in accordance with Equation (14) of Appendix A as well. For one load p per unit of thickness $L/8$ in from the corner the edge tension stress ($\theta = + 45°$) at $r = \frac{L}{2}$, Equation (14), would be $1.40\ p/L$. This is very nearly the maximum stress which occurs at $3.85\ t$, or $0.48\ L$ from the corner. For 2 loads, each p and $L/8$ from the corners, the top edge would deform in response to both loads and the total edge tension midway between the loads would be $2.80\ p/L$, or $1.4\ q$, somewhat higher than Guyon's value, Equation (18). Zero stress on the center section in accordance with Equation (14) would be $0.25\ L$ below the top edge. The total tension on the center section near the top edge between the 2 loads, each p , would be $0.35\ p$, very much greater than suggested by Guyon, but in substantial agreement with that shown in Reference (3) for single spans.

LIST OF CAPTIONS FOR ILLUSTRATIONS

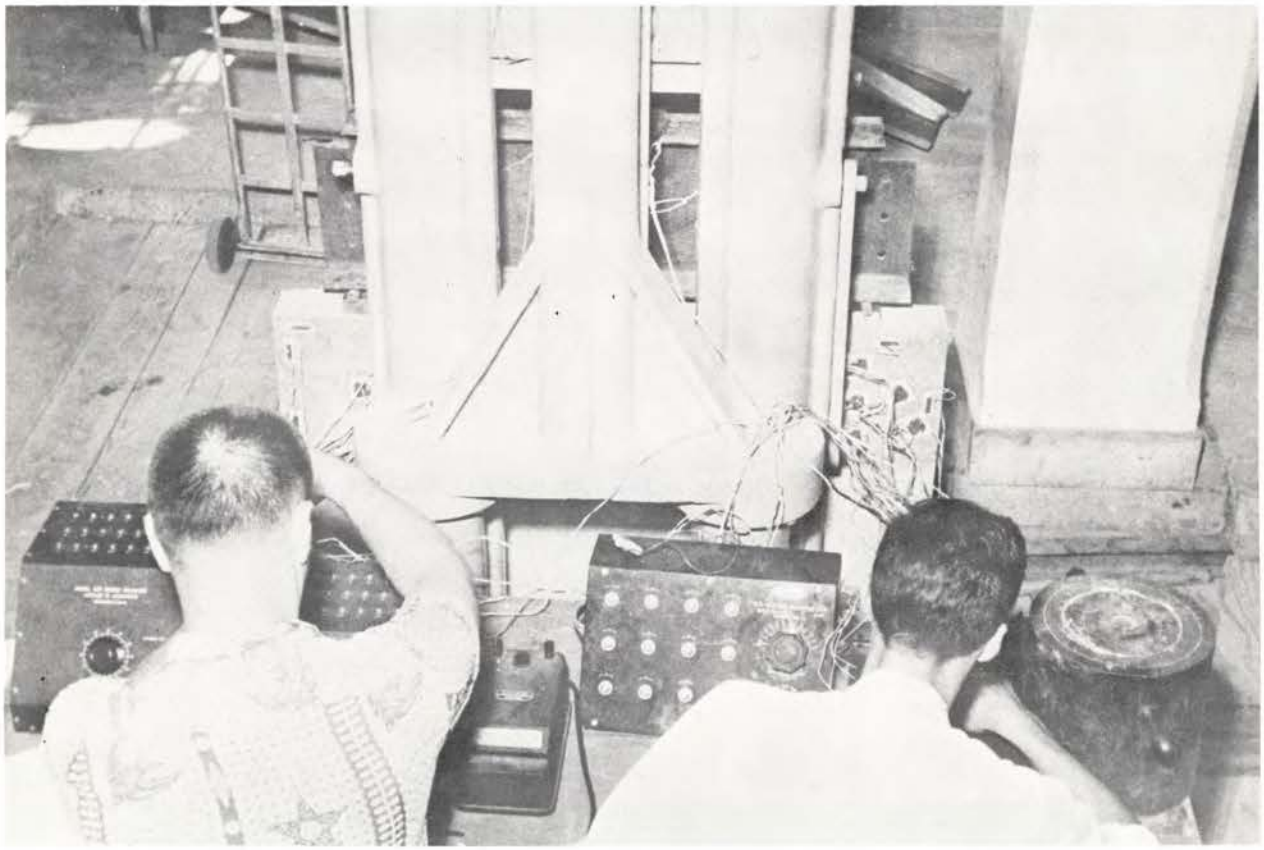

Figure 1. Short-time test specimen in place in testing machine for symmetrical loading.

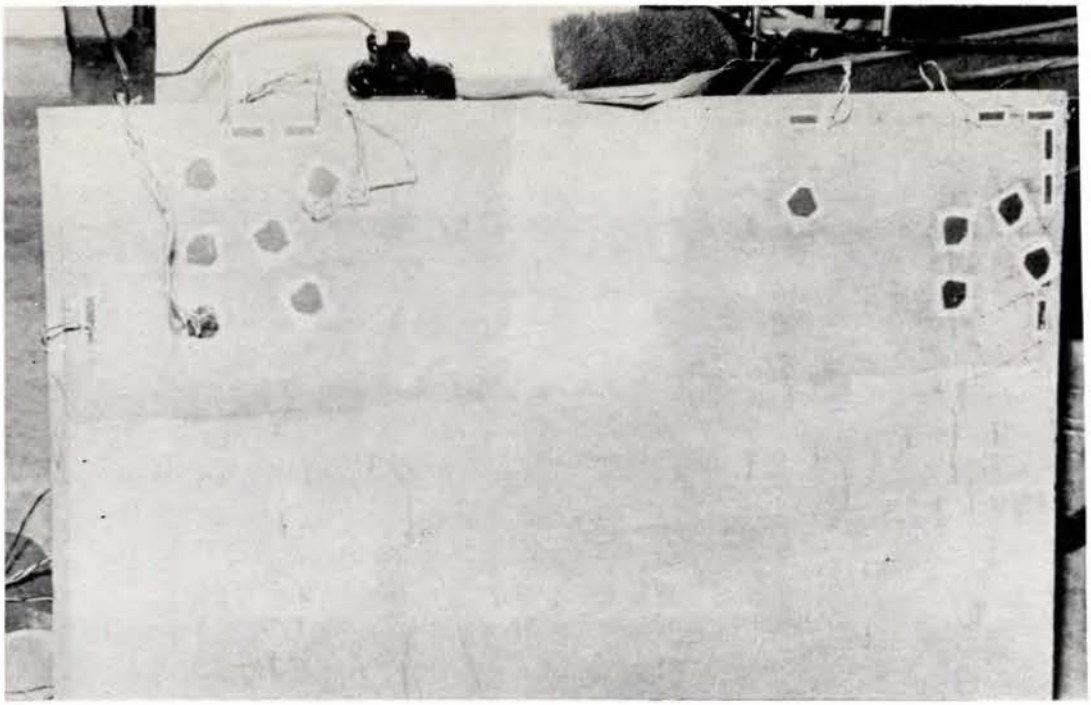

Figure 3. Placing of strain gages for symmetrical loading.

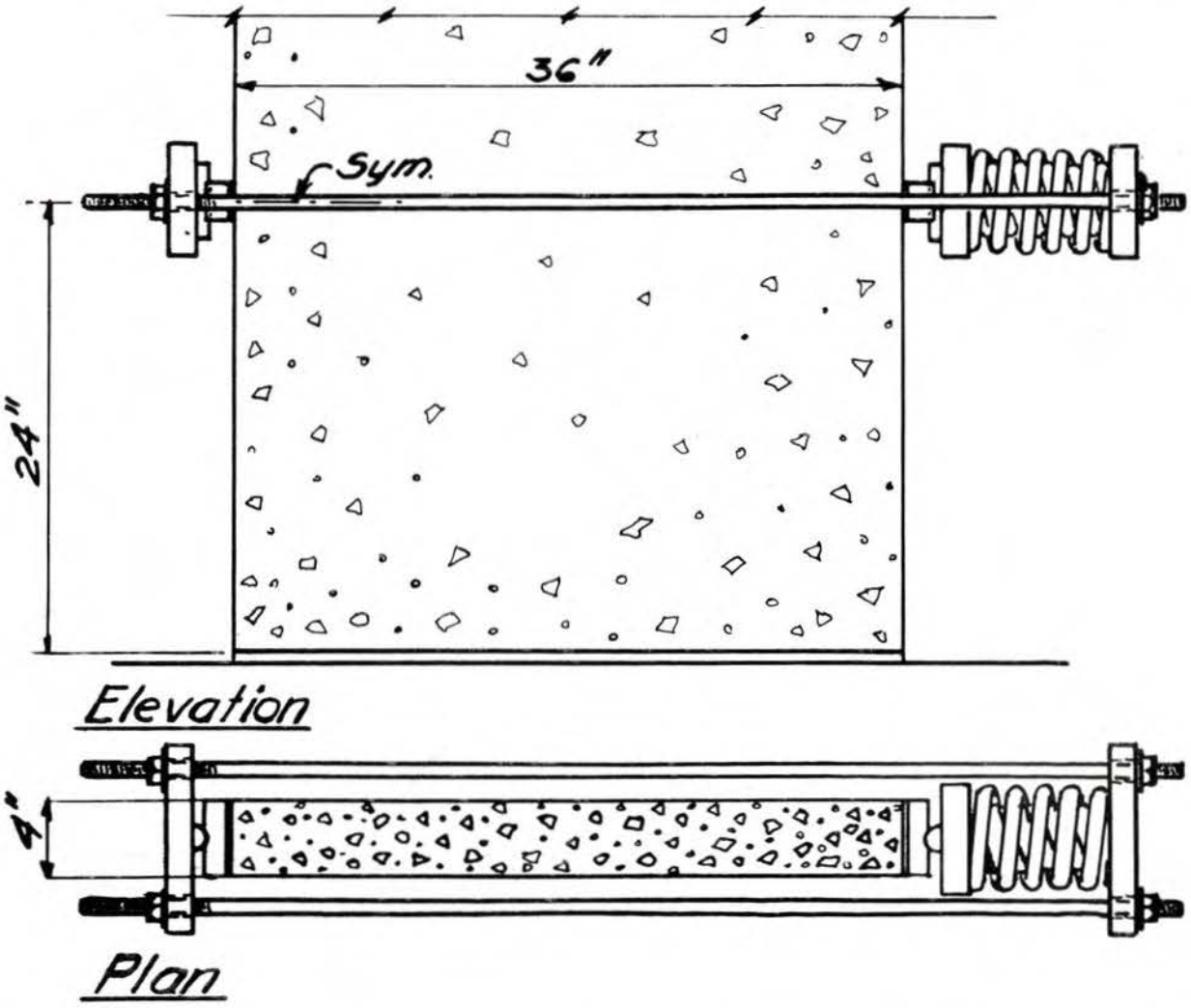

Figure 2. Loading arrangement for long-time tests, center load.

Figure 4

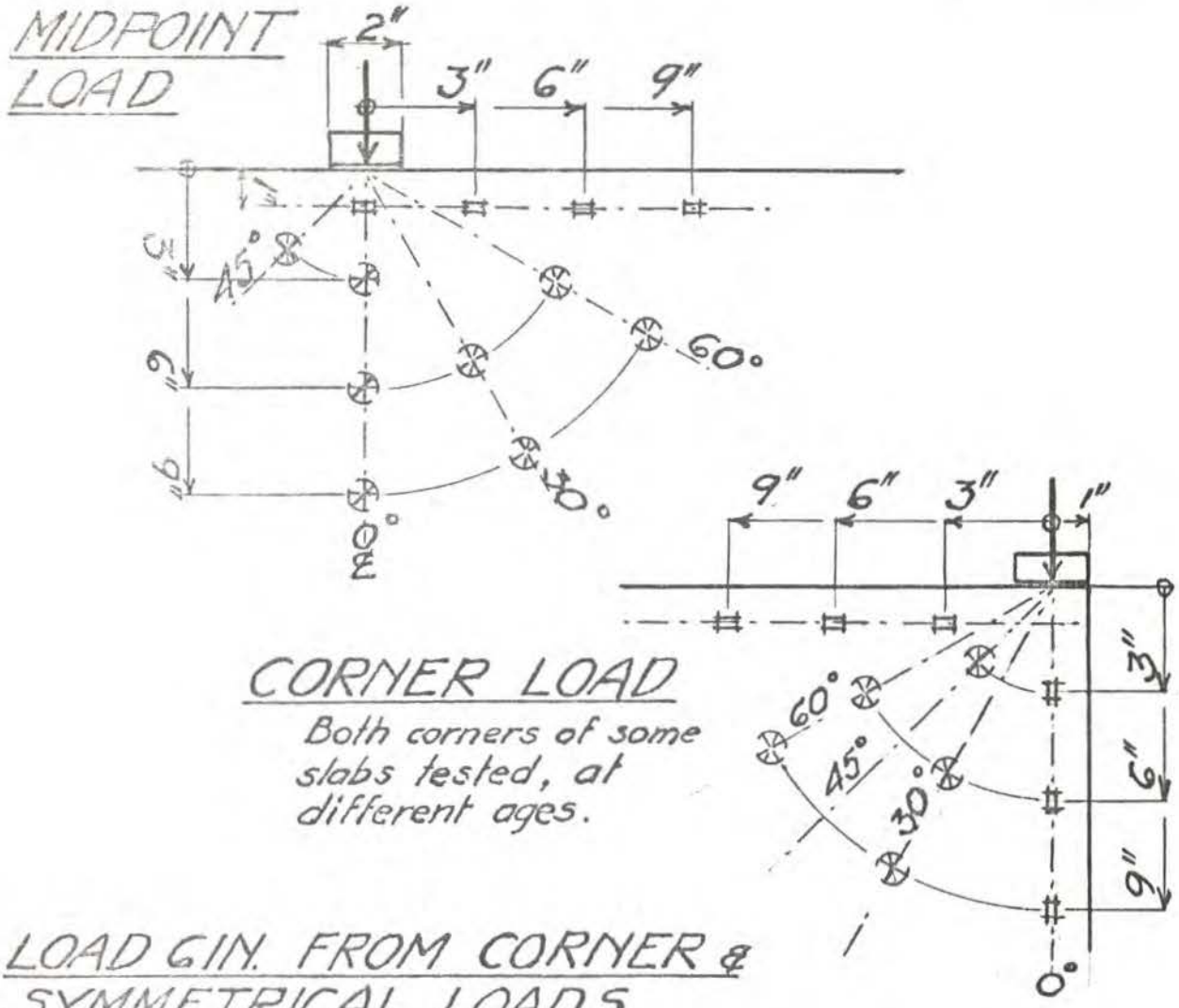
MIDPOINT LOAD
2"
3"
6"
9"
3"
6"
9"
45°
60°
30°
0°
CORNER LOAD
Both corners of some slabs tested, at different ages.
9"
6"
3"
1"
3"
6"
9"
60°
45°
30°
0°
LOAD 6IN. FROM CORNER & SYMMETRICAL LOADS
1"
3"
3"
6"
9"
15"
3"
3"
1"
1"
3"
6"
9"
45°
30°
45°
30°
0°
Linear strain
Strain rosette:
r – radial strain,
t – tangential strain,
d – diagonal strain.

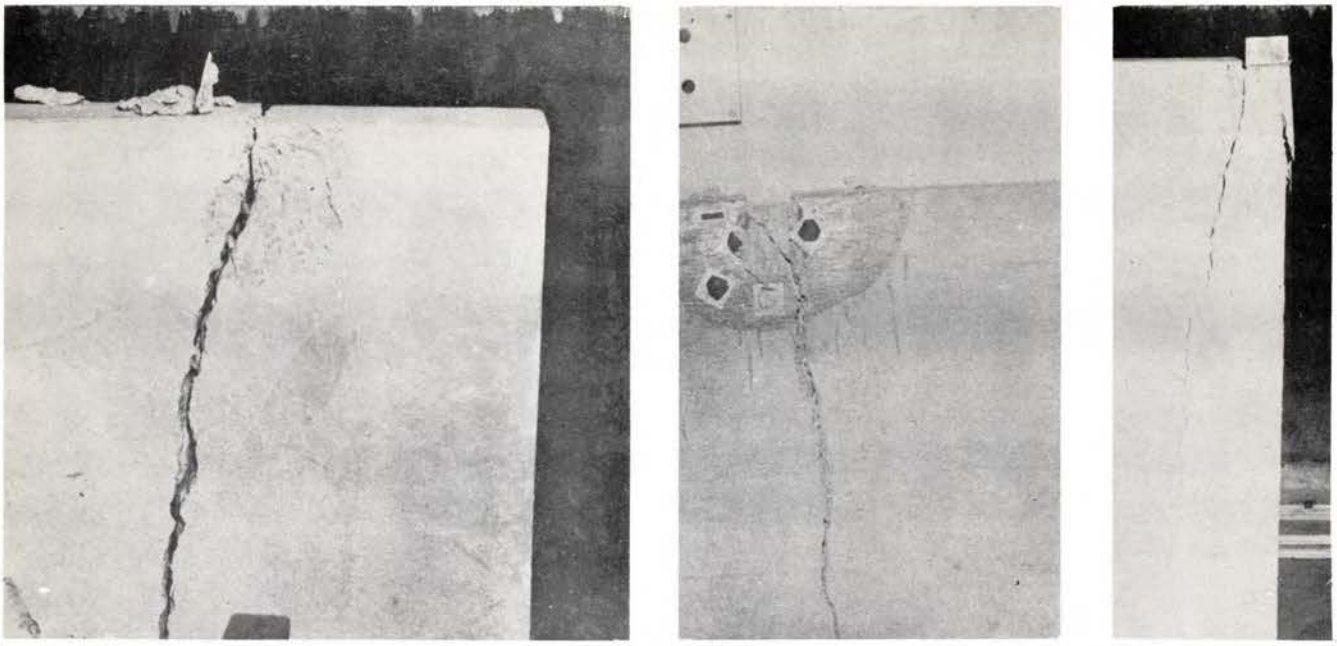

LOAD 6 IN. FROM CORNER CENTER LOAD CORNER LOAD

Figure 5. Typical test slab conditions failure.

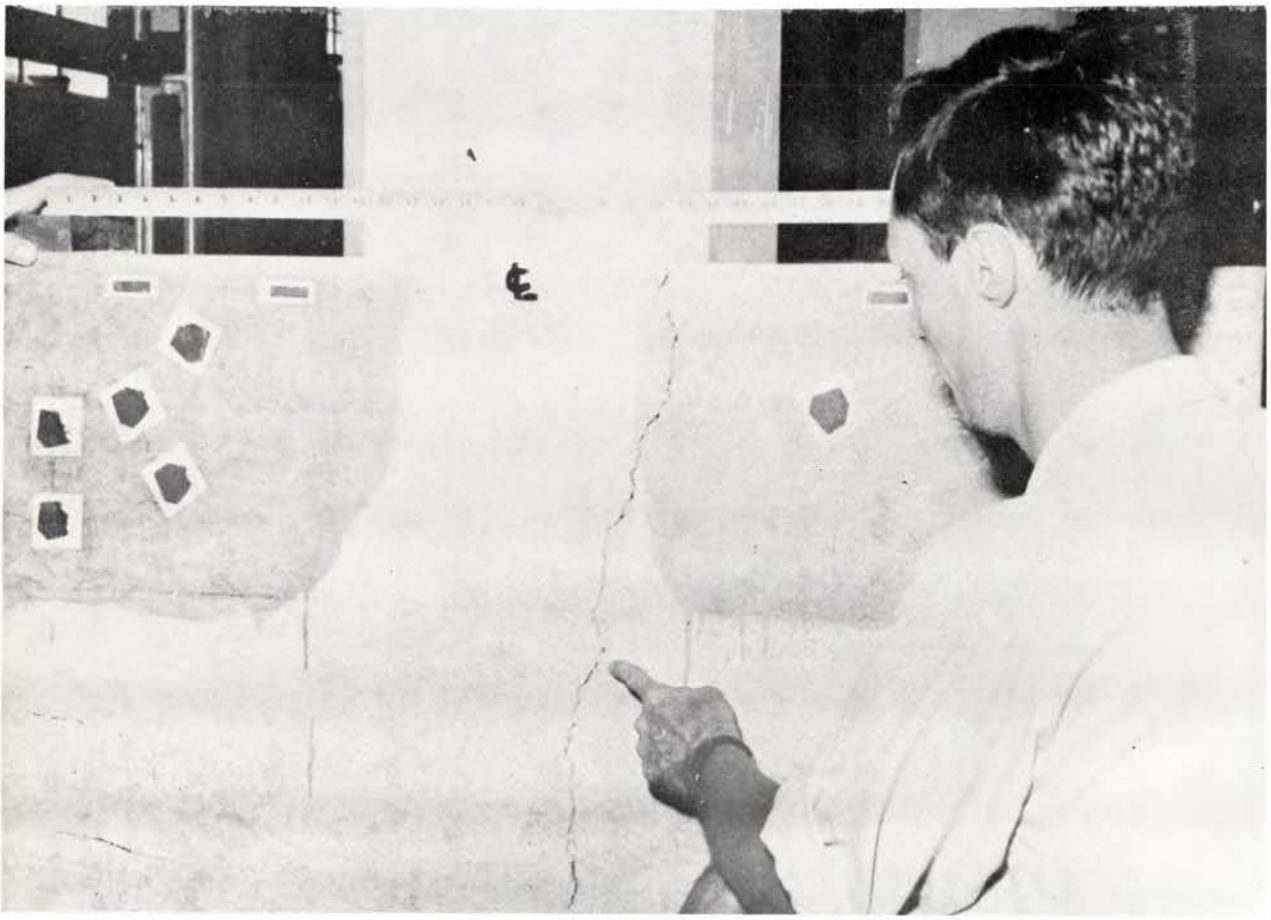

Figure 6. Typical failure between two symmetrical loads.

Figure 7

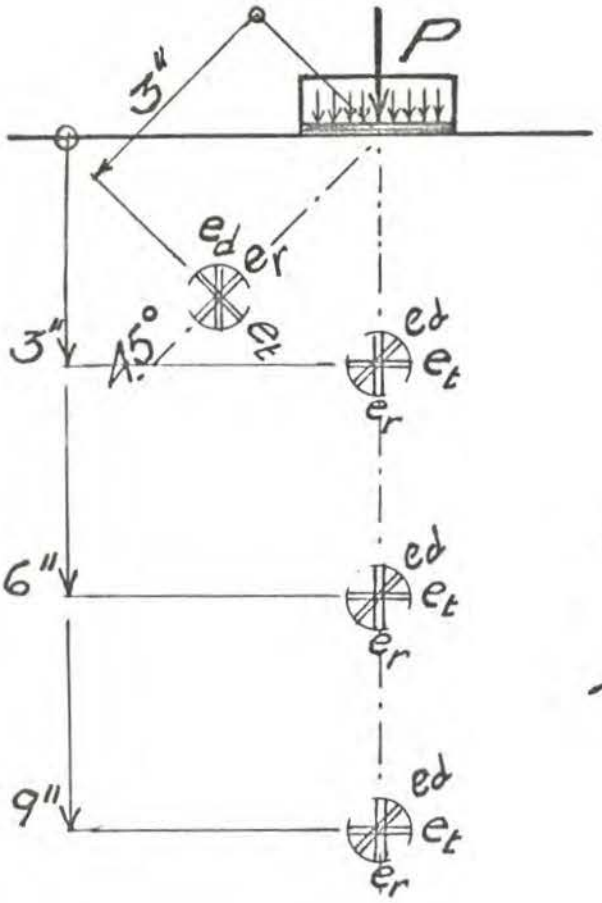

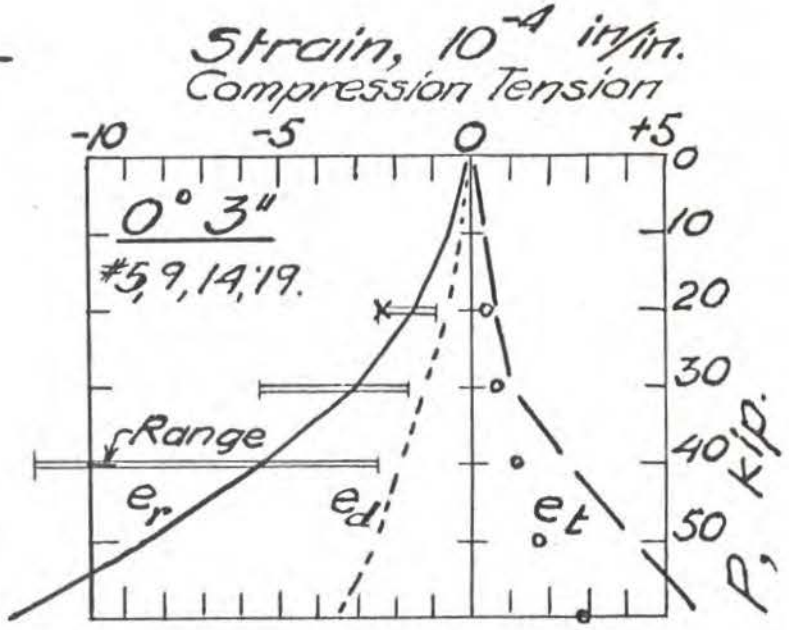

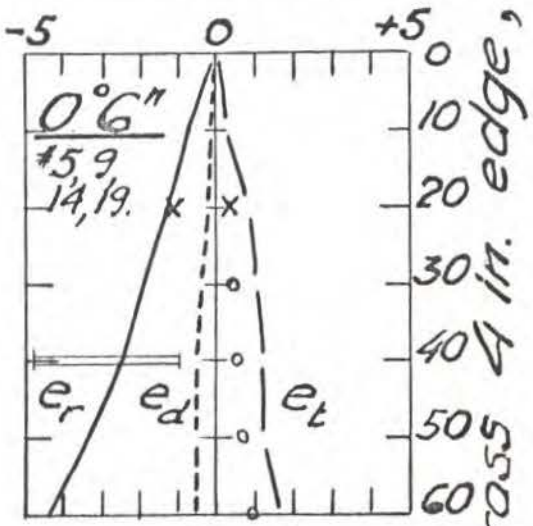

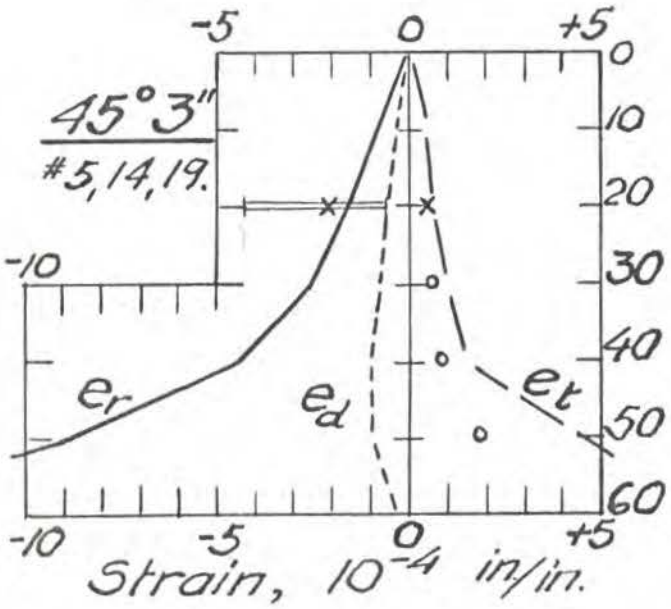

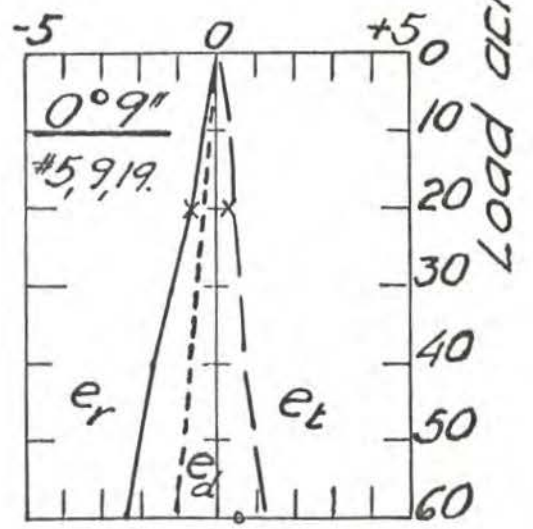

° Poisson's ratio 0.20

× Long-time test, at time of loading

Figure 8

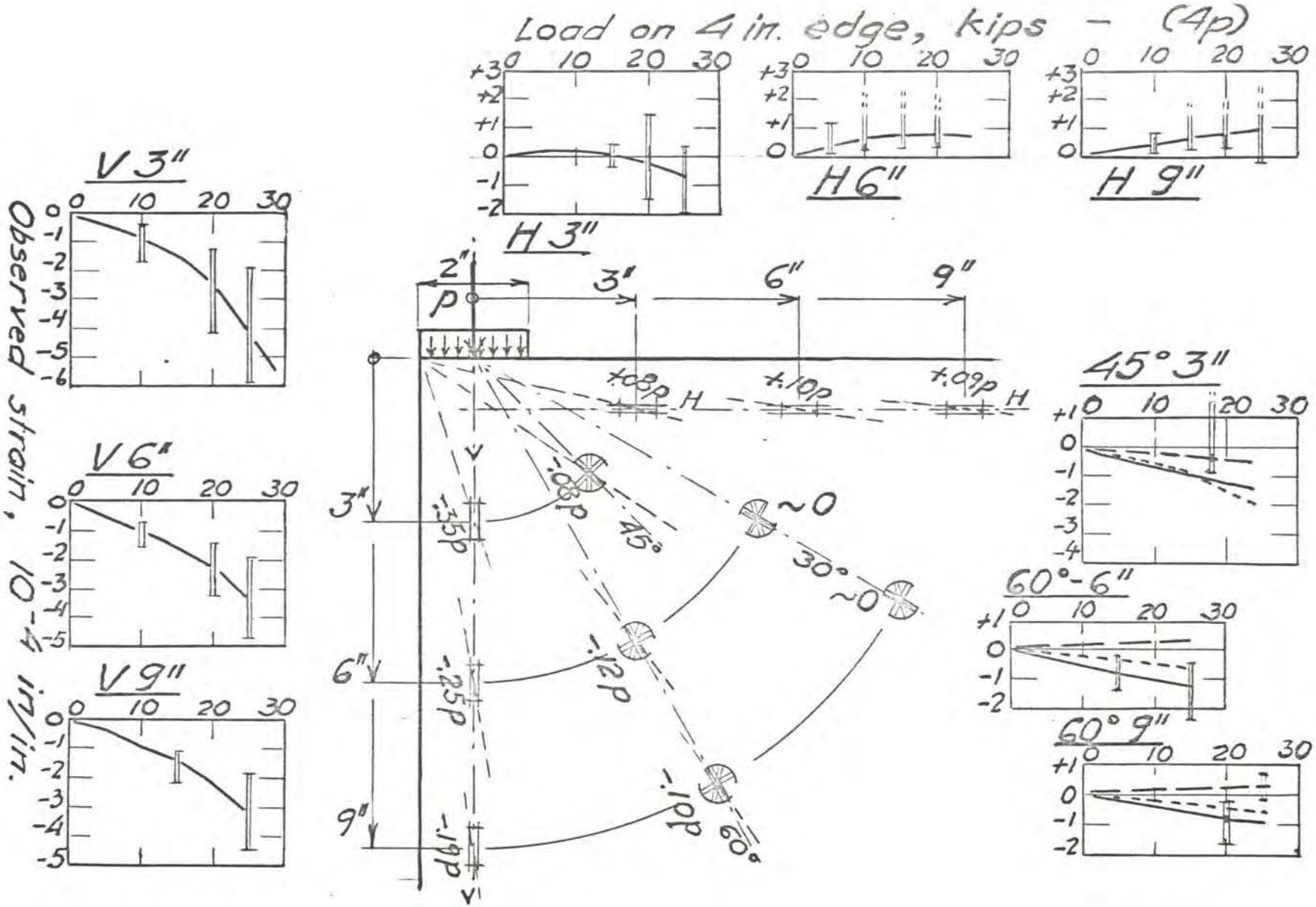
Load on 4 in. edge, kips – (4p)
H 3"
H 6"
H 9"
V 3"
V 6"
V 9"
Observed strain, in./in. ×10⁻⁴
45° 3"
60°-6"
60° 9"
2"
3"
6"
9"
P
+.08p H
+.10p
+.09p H
3"
6"
9"
-.03p
-.35p
-.12p
-.25p
-.10p
-.19p
45°
30°
60°
~0
~0

Figure 9

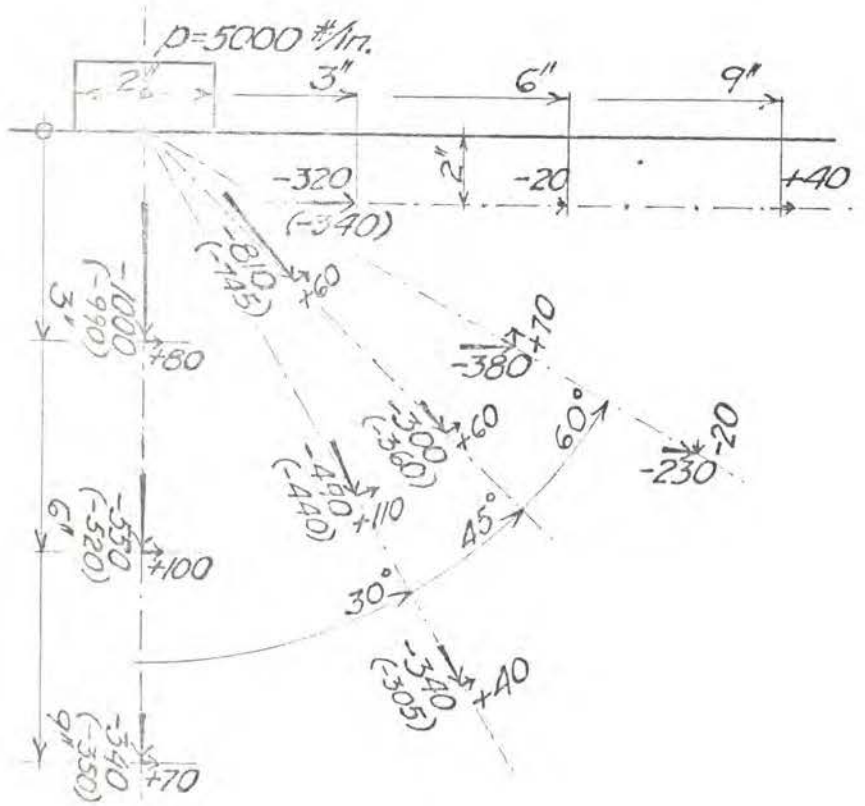

Figure 10

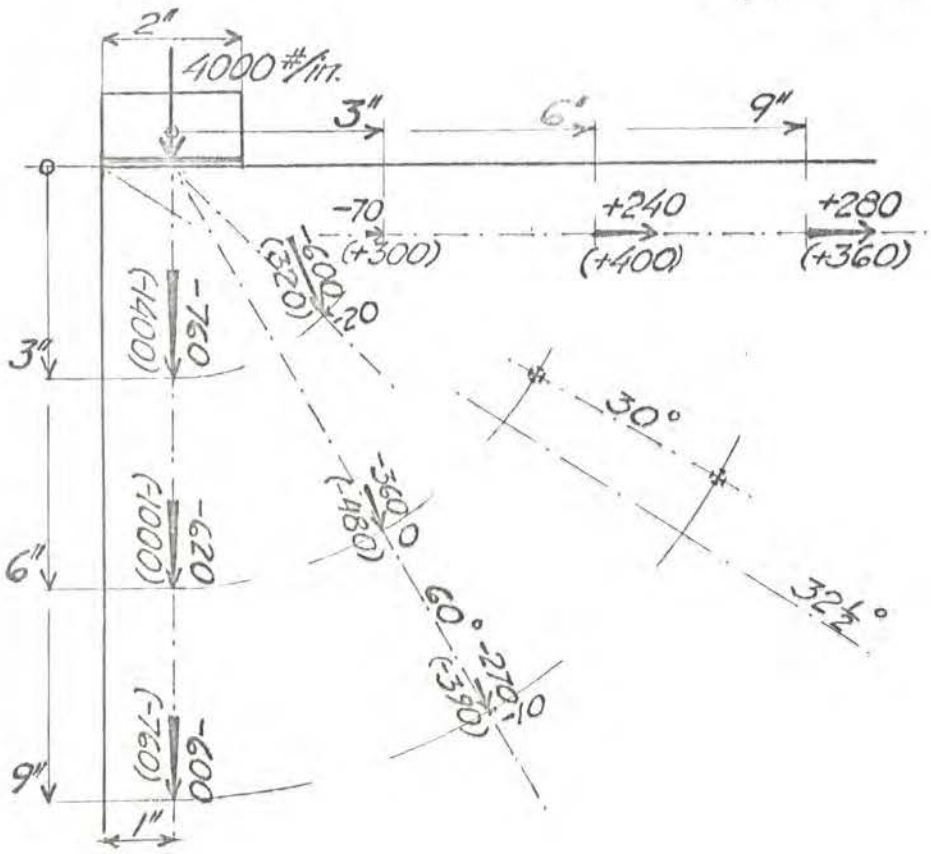

Figure 11

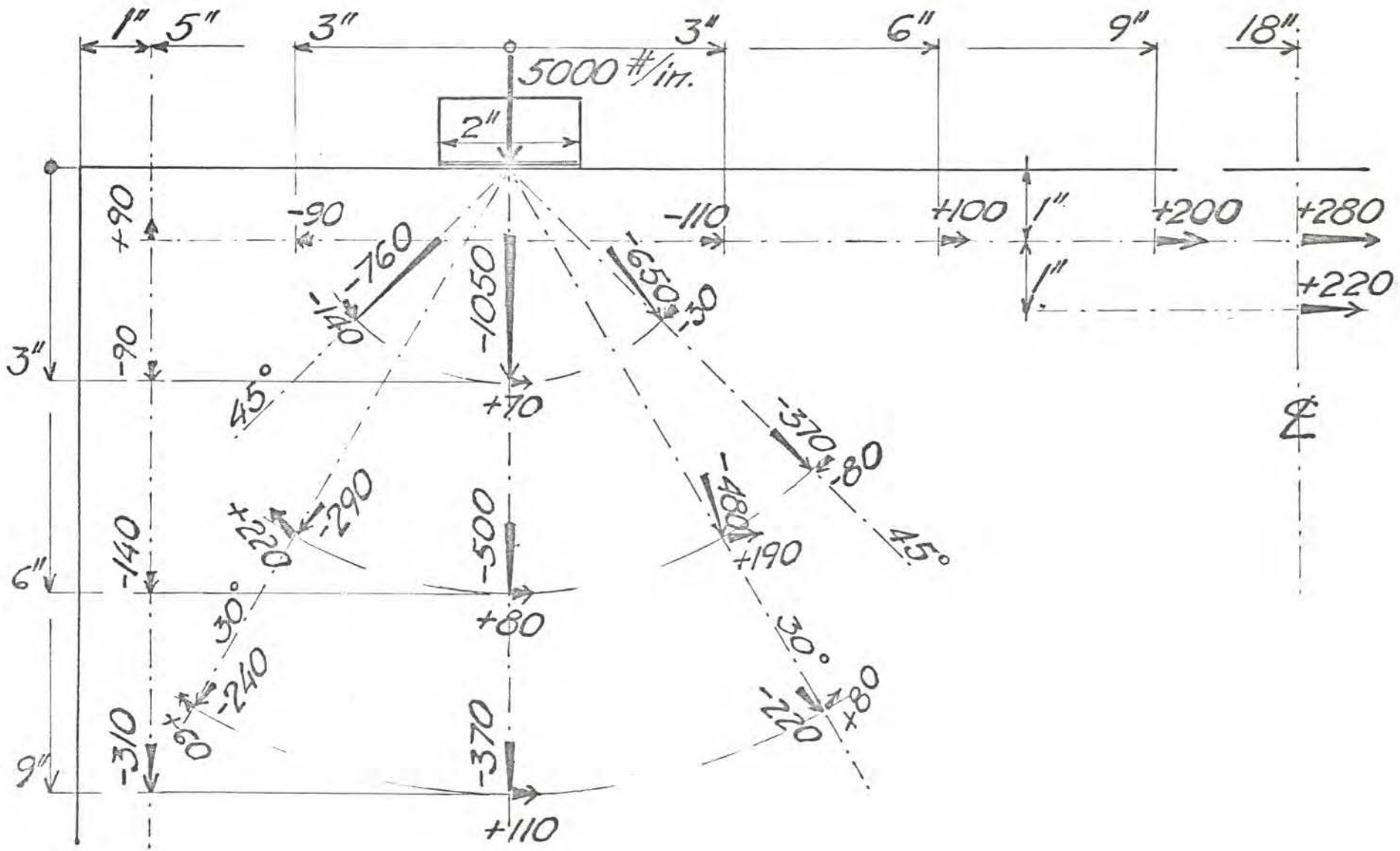
1"
5"
3"
3"
6"
9"
18"
5000 #/in.
2"
+90
-90
-110
+100
1"
+200
+280
+220
-760
-1050
-650
-30
-40
3"
-90
45°
+70
-370
-80
-290
+220
-480
+190
45°
-140
-500
6"
30°
+80
30°
-240
+60
-220
+80
-310
-370
9"
+110
℄

Figure 12

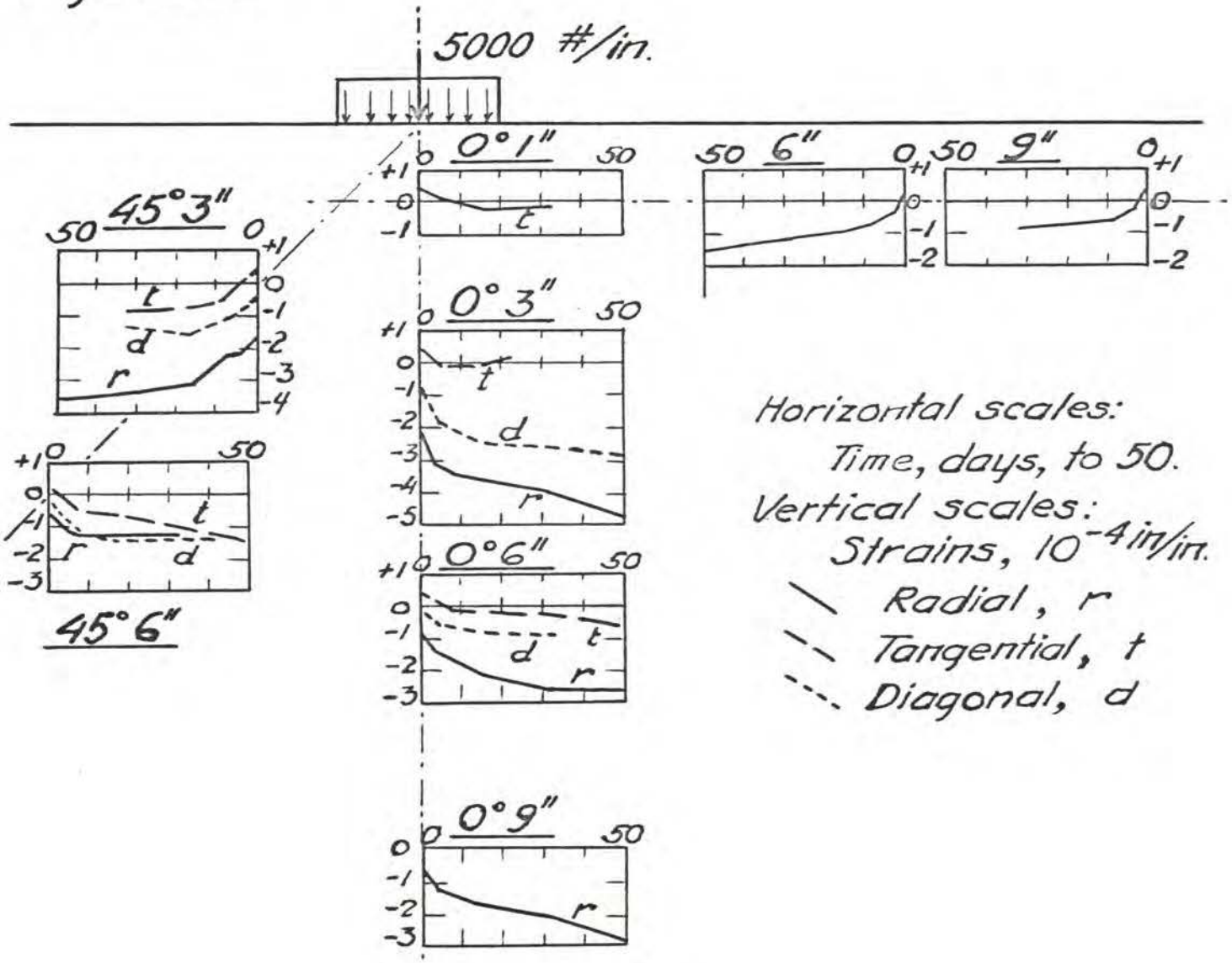
5000 #/in.
0°1"
6"
9"
45°3"
0°3"
0°6"
45°6"
0°9"
Horizontal scales:
Time, days, to 50.
Vertical scales:
Strains, 10^-4 in/in.
Radial, r
Tangential, t
Diagonal, d

Figure 13

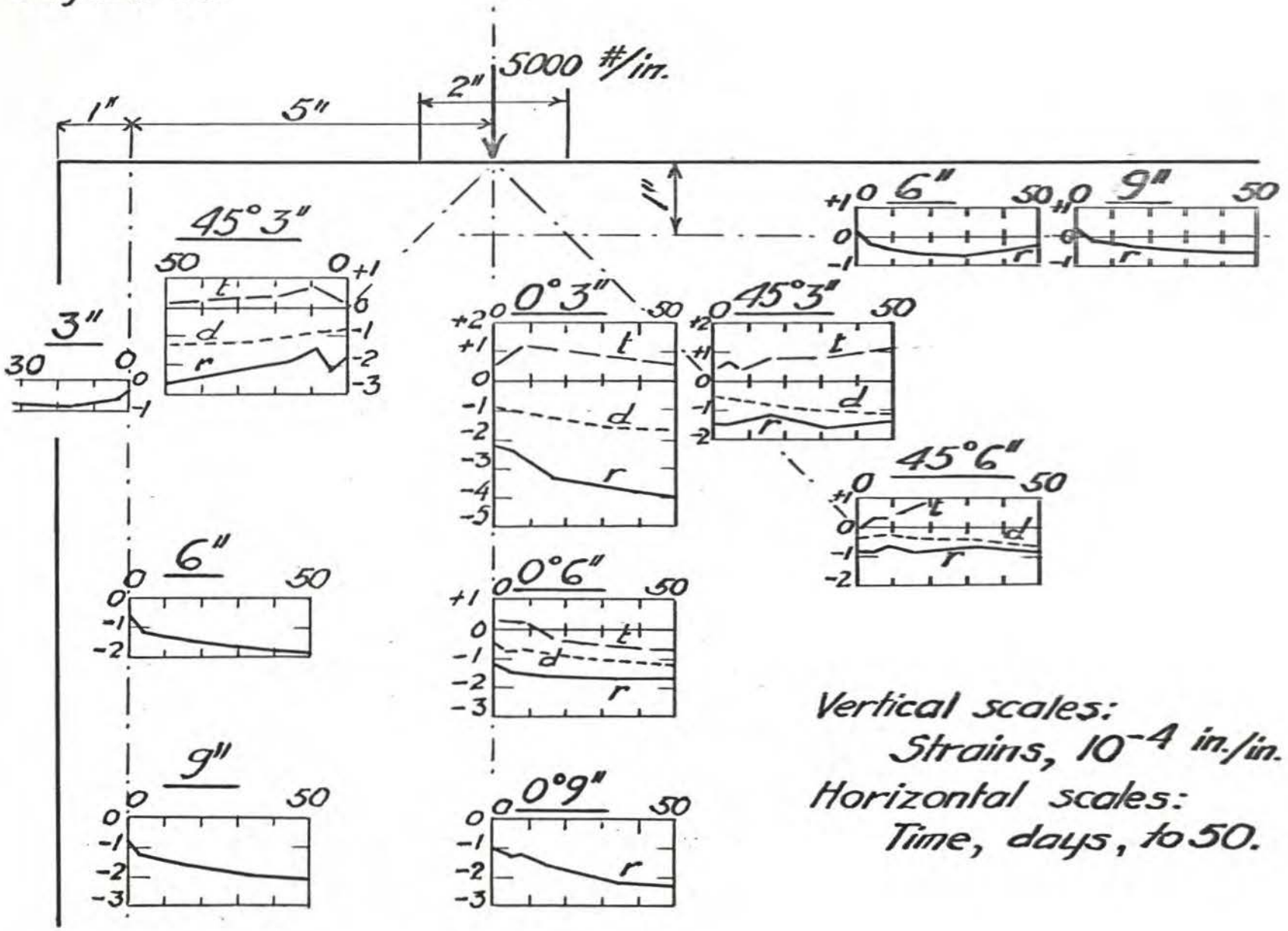
5000 #/in.
1"
5"
2"
3"
45° 3"
0° 3"
45° 3"
6"
9"
45° 6"
0° 6"
0° 9"
t
d
r
Vertical scales:
Strains, 10⁻⁴ in./in.
Horizontal scales:
Time, days, to 50.

Figure 14

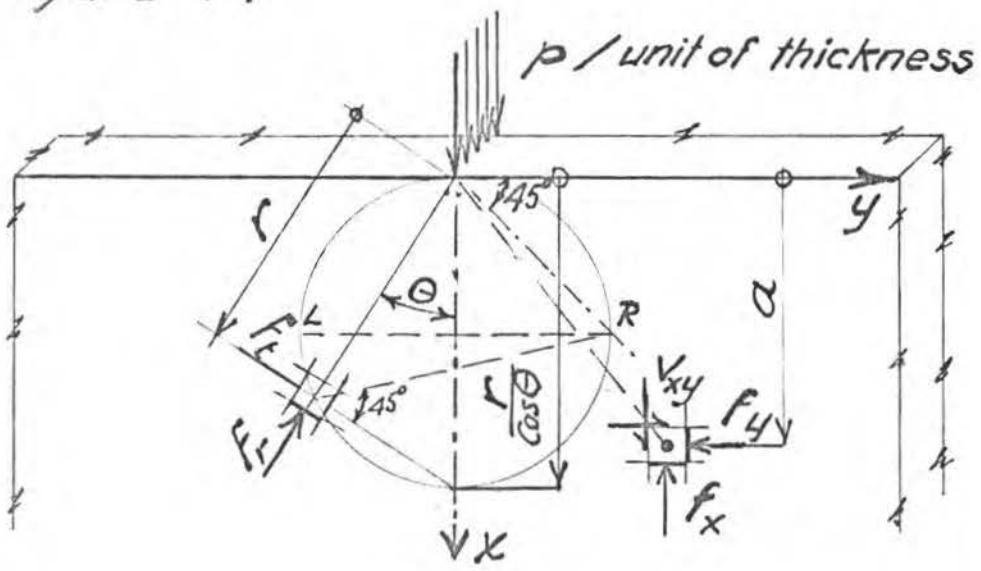

Figure 15

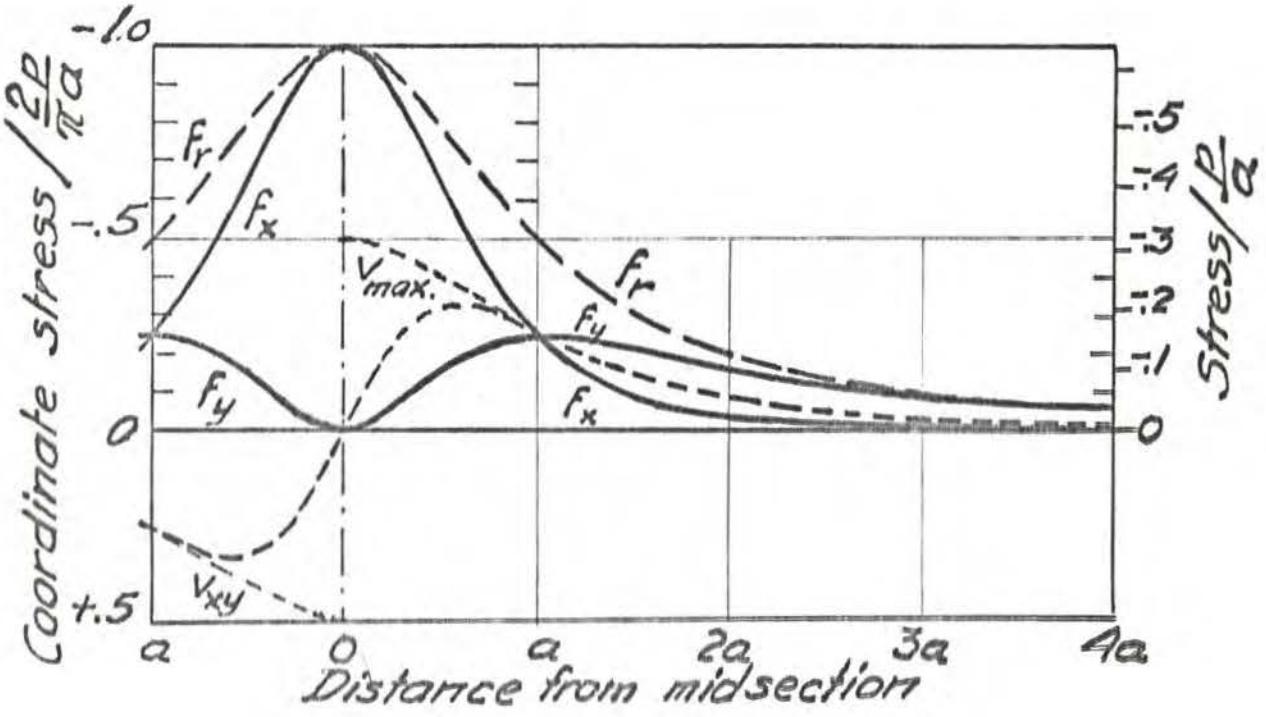

Figure 16

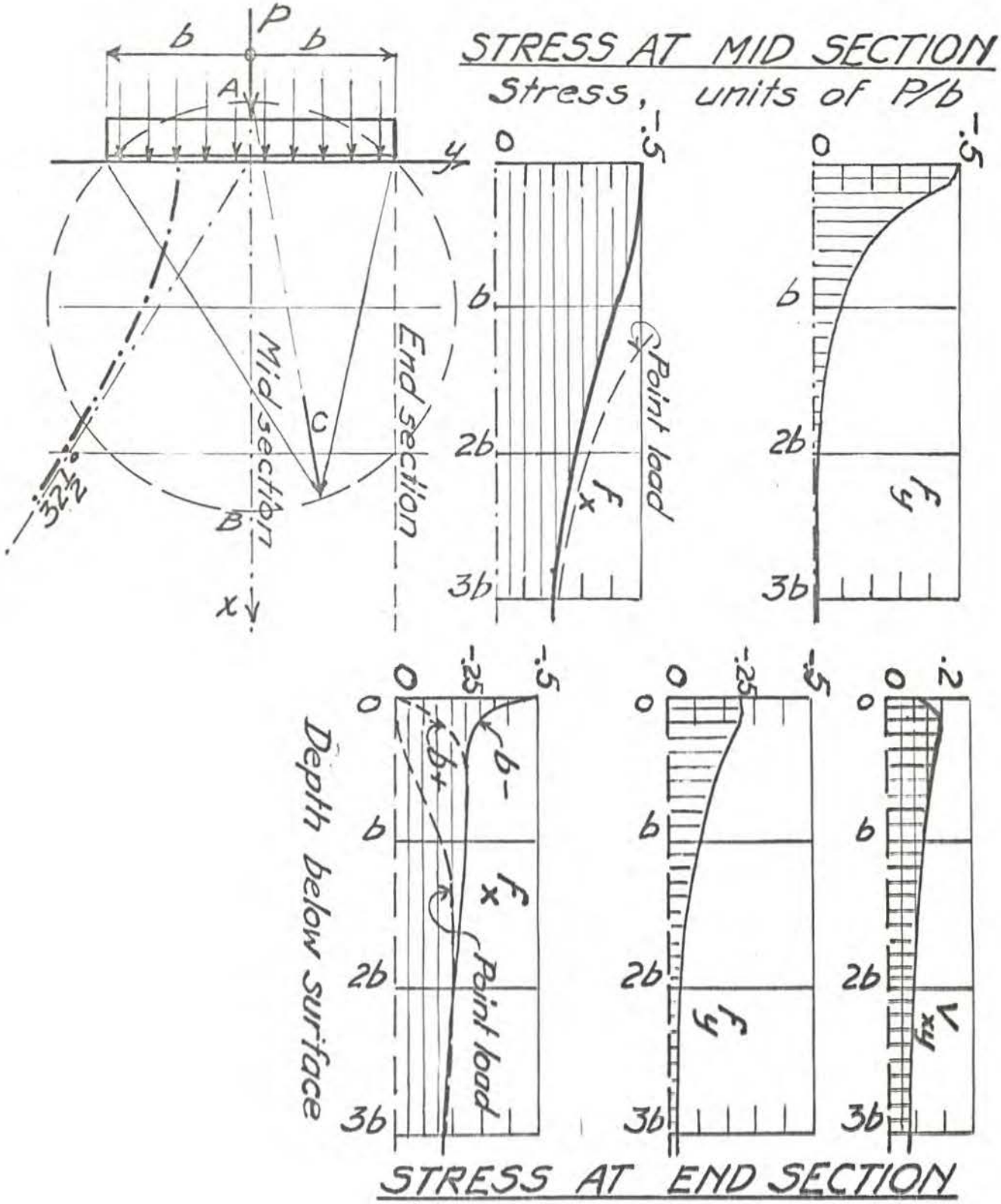
STRESS AT MID SECTION
Stress, units of P/b
b
P
b
A
y
x
Mid section
End section
B
0
-.5
b
2b
3b
Point load
f_x
f_y
-.25
.2
τ_{xy}
Depth below surface
STRESS AT END SECTION

Figure 17

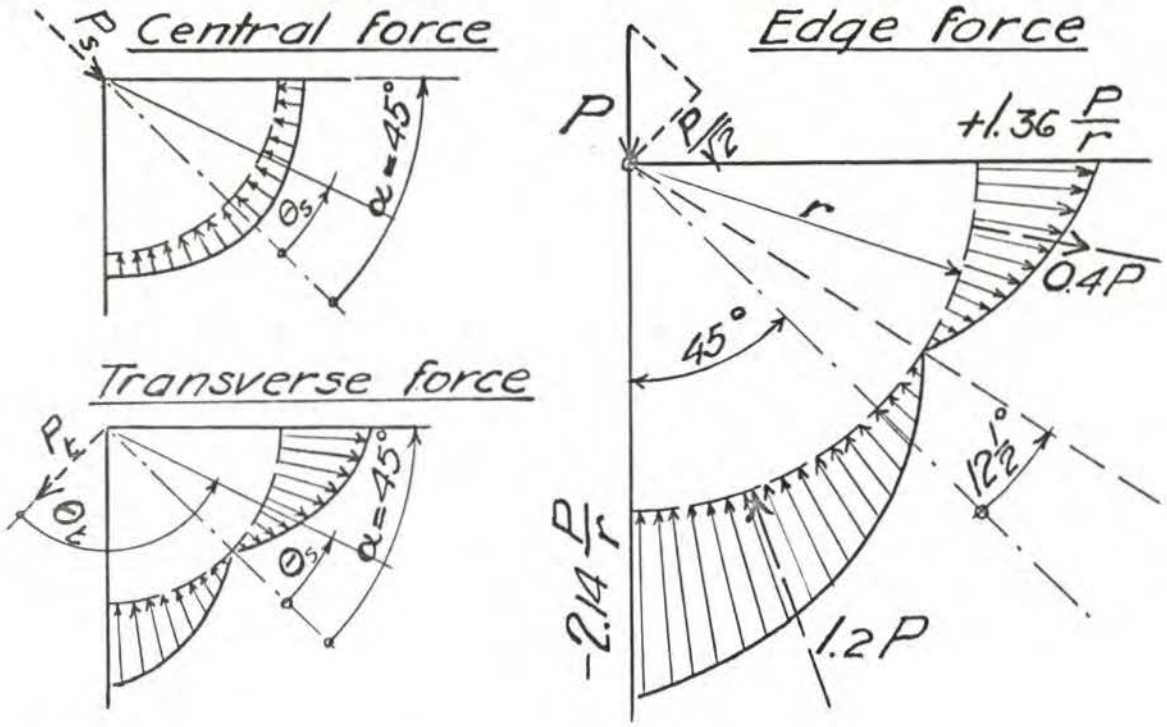

Figure 18

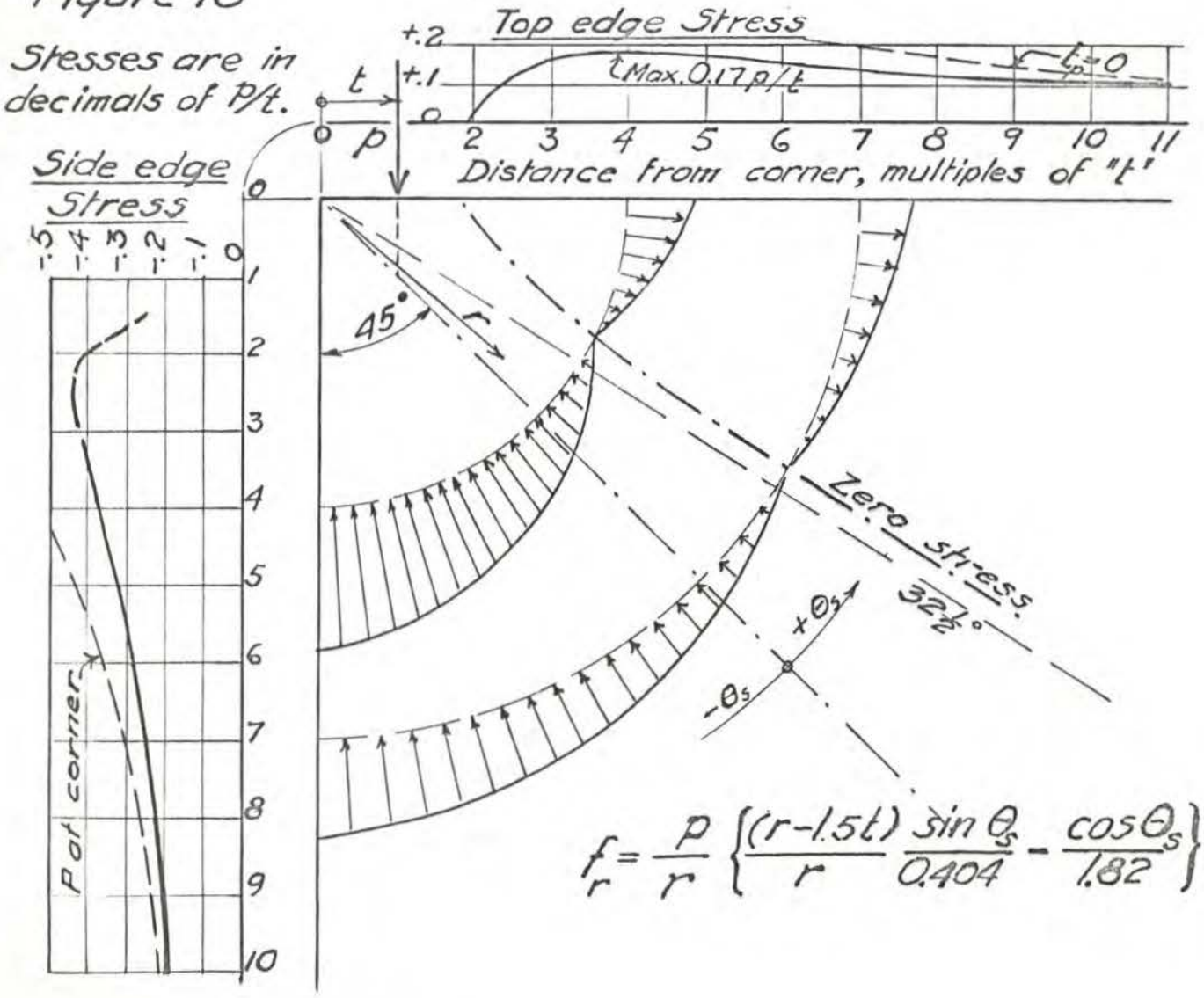

STRESSES AT MIDSPAN

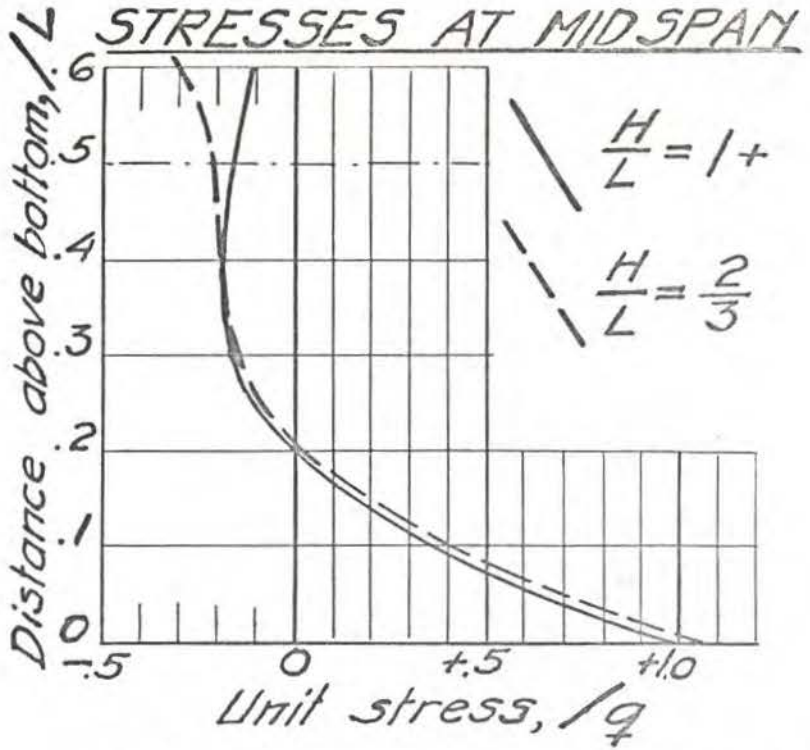

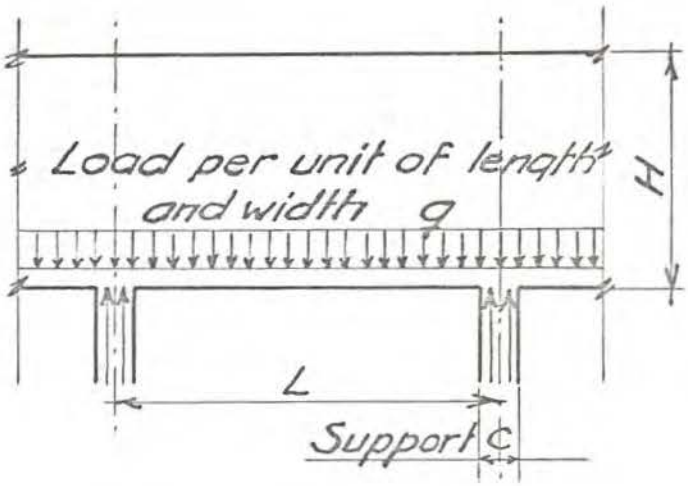

STRESSES AT MIDSECTION OF SUPPORTS

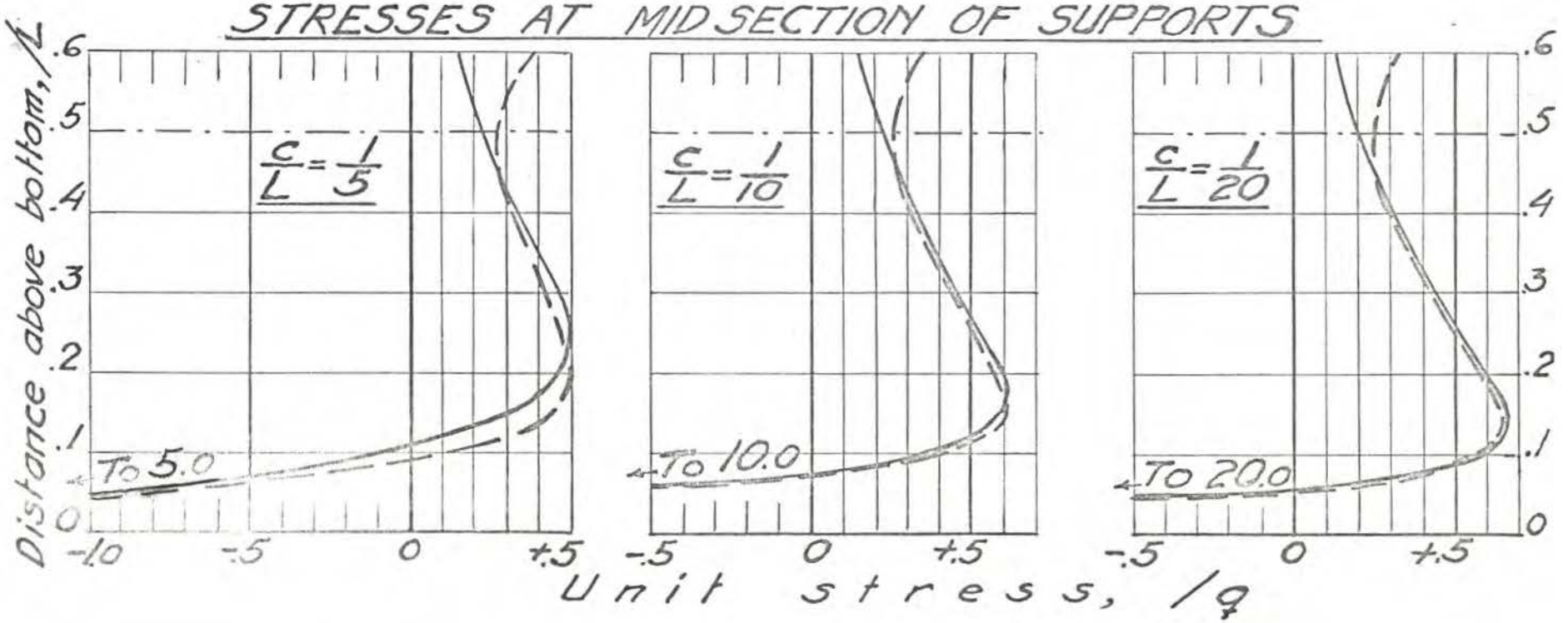

Figure 20

Figure 20a

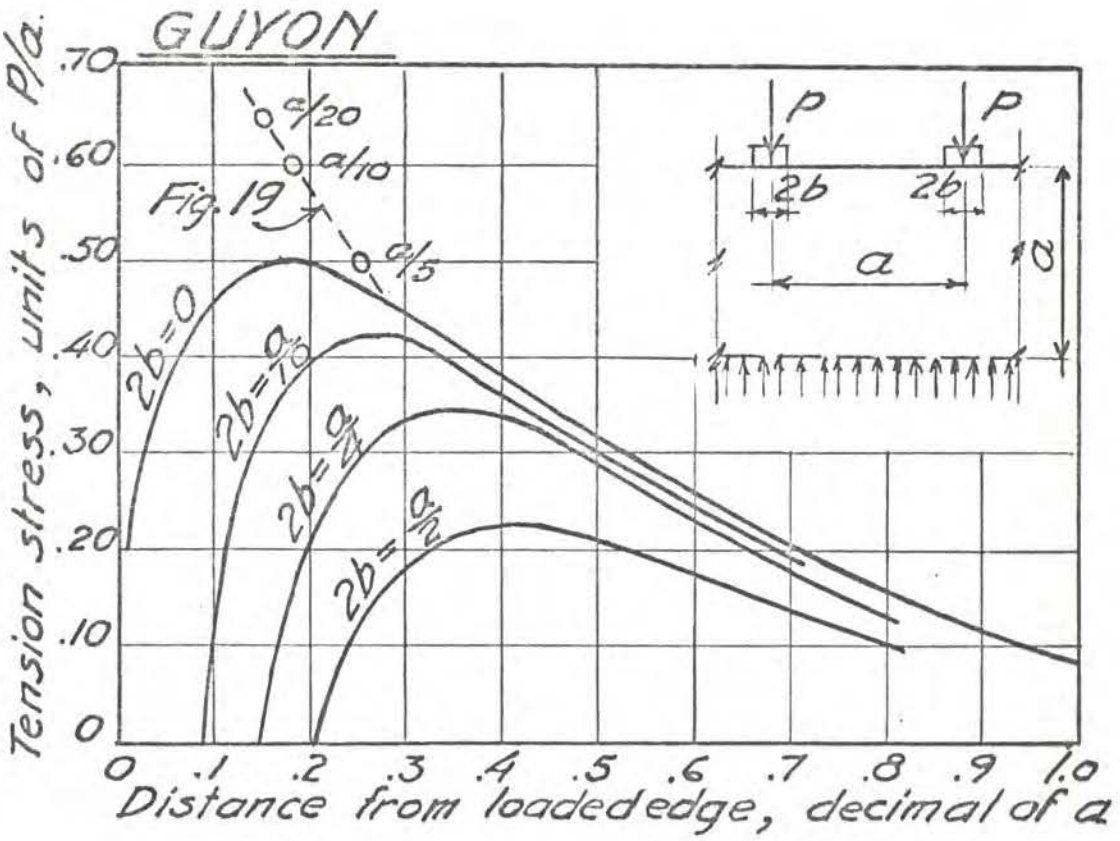

Figure 20b